
PERGAMON

Journal of the Mechanics and Physics of Solids
48 (2000) 827–865

JOURNAL OF THE
MECHANICS AND
PHYSICS OF SOLIDS

www.elsevier.com/locate/jmps

# Helical inclusion in an elastic matrix

L.I. Slepyan*, V.I. Krylov, R. Parnes

*Department of Solid Mechanics, Materials and Structures, Faculty of Engineering, Tel Aviv University, PO Box 39040, Ramat Aviv 69978, Tel Aviv, Israel*

Received 8 February 1999

**Abstract**

An elastic space containing an elastic helical rod subjected to both axial and radial extension as well as torsion is considered. Due to translation-rotation helical symmetry, the resulting elastic fields in the matrix can be expressed in terms of a two-dimensional helix-associated coordinate system. In this problem, a 'helical elastic foundation' as a generalization of the Winkler foundation is determined by means of which the interacting force and moment at the rod/matrix interface can be expressed in terms of the rod displacement. The matrix is assumed to be linear elastic while the geometric nonlinearity of the helical rod is taken into account. Using superposition of fundamental solutions for a homogeneous elastic space (in the absence of the rod), and the constitutive and equilibrium equations for the rod, the internal forces and moments in the rod as well as the displacement and elastic fields in the matrix are obtained. Along with the general results, two asymptotic solutions are presented. The first, corresponding to a small curvature but not too small pitch, allows an analytical integration of the rod–matrix interaction over the rod cross-section boundary. The second corresponds to an almost straight helical rod: the helix becomes a straight line, but in the limit the main normal to its axis describes a screw surface as in the case of a 'genuine' helix. In this case, the helical elastic foundation has a closed-form parametric expression which is valid for a rather large range of the helix parameters. The foundation stiffness is found as a function of the helix pitch and the rod radius; the problem thus is reduced to a system of finite, nonlinear equations. 

*Keywords:* A. Strengthening mechanisms; Stress concentrations; B. Constitutive behavior; Fiber-reinforced composite material; C. Asymptotic analysis

* Corresponding author. Tel.: +972-3640-6224; fax: +972-3640-7617.
*E-mail address:* leonid@eng.tau.ac.il (L.I. Slepyan).

0022-5096/00/$ - see front matter 
PII: S0022-5096(99)00049-6

## 1. Introduction

From the point of view of their diverse applications, composites based on curvilinear inclusions possess considerable advantages in comparison with straight-fiber composites. The former can be more extensible and flexible and provide for a greater controlled variation of the mechanical features of the composite. In particular, for this reason, ropes and cables are usually fabricated as an assembly of helical strands. Since curvilinear reinforcements lead to a hardening type nonlinear stress–strain relation, this provides for an increased stability of the material under extension thus leading to an essential increase of energy absorption of the material before rupture (Cherkaev and Slepyan, 1995). It is one of the most important features of such a composite. If the structure is properly chosen, stable extension continues even during progressive fracture of the matrix. A simple model of such a process is presented below.

Among such structures, composites based on helical inclusions deserve special attention. The helix, having two free geometric parameters, is a unique perfect curve with uniform curvature and torsion which, for the case of a single helical inclusion in an isotropic matrix (or in the case of a set of coaxial helices of the same pitch and direction of rotation), leads to helical symmetry and thus presents a unique possibility to examine the main phenomena based on a relatively simple model. Owing to uniformity, translation-rotation symmetry holds, which leads to the existence of simple states of the composite. In such a state, the stress and strain fields appear invariant to an observer moving and rotating with the triad natural to the helix. In this connection, note that a composite with a spatial helix represents a two-dimensional problem, while a plane curvilinear fiber leads to a three-dimensional problem.

Composites based on plane curvilinear fibers and layers were considered by Kagawa et al. (1982), Chou (1992), Chiskis et al. (1997) and Chiskis and Parnes (1998). Dynamic fracture behavior of helical fiber metal–matrix composites was experimentally studied in Kagawa et al. (1982). It was shown that initial twisting of the fiber increases the ductility of the composite. Fairly larger ultimate tensile strains were obtained at a small expense of ultimate tensile stresses. Composites with helical symmetry were also considered in Iwata et al. (1994), Li et al. (1994), Kohkoner et al. (1991). Delamination of a helically reinforced composite was experimentally investigated by Foral (1989). The mechanics of helically wound materials was studied by Morris and Harris (1989) and Kautz (1987). Some devices of thermal energy storage systems include a helical heat exchanger embedded in a soil (Rabin and Korin, 1996) which can be considered in the framework of the helical inclusion theory. Helical elements have also been used as soil stabilizers (Shewbridge and Sousa, 1991). Many applications of single- and multi-helix structures for medical purposes are shown in the Handbook of Coronary Stents (1997).

It should be mentioned that along with the problem of a composite material with helical inclusions, helical systems are relevant to a wide variety of fields in different areas of science and engineering, from mechanical properties of helical

DNA molecules and chiral polymers to mechanics of reinforced concrete, large-scale spatial structures, deployable antennas, etc. Note that helical symmetry of mechanical properties arises not only due to the corresponding inclusion. For example, as shown in Lhermitte et al. (1989), some types of cross-ply reinforced composites exhibit helical symmetry on the microlevel. Further, it is known that some polymers develop helical properties on the microlevel during polymerizations (Fujiki, 1996; Meille and Allegra, 1996; Okamoto and Nakano, 1996). We present below several types of systems related to this 'helical topic'.

Helical structures are very common in biological systems. It was recently found that some bones possess a helical organization of their structure (Petryl et al., 1996). A special class of biological objects with helices is represented by the DNA molecule which is known as a double helix. Mechanical properties of such a helix are of interest (Bustamante et al., 1994; Kobe and Wiest, 1993; Smith et al., 1992). In addition, some medical devices (for example, micro-pumps) embedded in a bio-medium have helical structure (Dong et al., 1996; Pathak and Singh, 1996). Helical microstructure also has an influence on the mechanical properties of wood (Navi and Huet, 1989).

Many structural elements used in engineering practice can be considered as helical composite structures. The best known example, as mentioned above, is a cable consisting of a number of helical strains. The mechanics of such a cable has recently been studied intensively (Cardou and Jolicoeur, 1997; Zhang, 1997; Grum-Grzhimajlo et al., 1995; Williams et al., 1993; Ergashov, 1992). Helical strands are also used as reinforcements for tubes and flexible pipes (Butterworth, 1992; Breig, 1991; Savenkov and Solodova, 1988). In Shen et al. (1997), a helical constrained layer was shown to be useful as an actuator for longitudinal-torsional vibration control of shafts.

Some classes of solutions relevant to the dynamics of a helical string were recently obtained. An exact analytical solution describing solitary waves in an inextensible helical fiber was obtained in Slepyan et al. (1995a). Some numerical results of the problem were presented in Slepyan et al. (1995b). This solution was then extended to the case of an extensible helical string of an arbitrary nonlinear elastic material (Slepyan et al., 1998). Solitary waves in the helical string, rotating at infinity as a rigid body, were thereafter considered in Krylov and Rosenau (1996). A complete traveling wave solution describing all possible types of periodic and solitary waves in an inextensible fiber was obtained in Krylov et al. (1998). Finally, it was shown that axial dynamic tension of a helical thread leads to an extraordinary nonstationary binary wave (Krylov and Slepyan, 1997).

This topic is not exhausted by mechanical problems. Electro-magnetic-wave-propagation conductors preshaped into a helix are widely used, especially as antennae. This kind of device has long been in use (Watkins and Ash, 1954). Some recent results can be found in Padros et al. (1997) and Pistol'kors et al. (1995). A large number of works are devoted to the study of so-called chiral media. Such a medium can be represented by a composite containing helical conductive or dielectric fibers embedded in a matrix. As a result, the composite

possesses helical symmetry in its electro-magnetic features. This has been studied by Lindell et al. (1994), Mariotte et al. (1996) and Ge et al. (1996).

In the present work, uniform axial and radial extension and torsion of the matrix perturbed by the helical inclusion are studied. The work falls within the field of the mechanics of heterogeneous materials (Aboudi, 1991; Christensen, 1979; Hashin, 1983). The main goals are (a) homogenization of the helix-inclusion composite, that is, the determination of additional global stiffnesses introduced by the inclusion; (b) a derivation of the main asymptotes which describe the inclusion/matrix interaction, thus leading to the determination of a 'helical elastic foundation' as a generalization of the Winkler elastic foundation and (c) estimation of the inherent scales of the local, inclusion/matrix interaction stress fields.

In this paper, the main solutions from uniform strains of an elastic space perturbed by a unique, elastic helical inclusion are derived. Due to translation-rotation helical symmetry these solutions are two-dimensional in a helix-associated coordinate system: they are independent of the coordinate along the rod axis.

The inclusion is considered to be a helical rod whose behavior is governed by geometrically nonlinear equations. Elongation of the rod is taken into account along with its bending and torsion while lateral shear is neglected. In accordance with the equations for the rod, only integral values of the rod–matrix interaction, namely the normal force and moment, are considered. The Fourier components, self-equilibrated at the rod cross-section are not taken into account nor is stability of the helical rod under compression and the decreasing-helical-angle torsion of the composite considered.

The radial displacement and the rotation of the rod cross-section as well as the rod–matrix-interaction radial force and moment are derived. In determining the stress and strain fields in the matrix, the 'method of imaginary sources' is used. These fields are represented using superposition of the fundamental Kelvin solutions corresponding to a homogeneous elastic space (in the absence of the rod) subjected to a concentrated force and a concentrated moment. Displacement and strain fields are calculated as functions of unknown distributions of these forces and moments along the deformed rod axis. Making use of compatibility at the rod/matrix interface, the proper distributions are found which lead to the actual stress and displacement fields in the matrix as well as the internal forces, moments and displacements of the rod.

Numerical results of the solutions are presented to show the influence of the helix parameters and the ratios of the matrix-to-helix elastic moduli. The stress fields in the matrix due to the rod/matrix interaction are shown to decay rapidly outward from the rod. In essence, they exist in a surrounding-rod layer of the order of the rod radius.

Along with the general results, some asymptotic solutions are presented. The first corresponds to the condition when the curvature of the helix is small and the angle between the helix and its axis, the 'helical angle' is not too close to $\pi/2$. In this asymptote, the helical foundation is represented by a single-integral

parametric expression while in the general case it has a double-integral representation.

The second asymptote corresponds to a small helical angle and helix radius, such that the helix approaches a straight line, but the normal to its axis forms (in the limit) a screw surface as in the case of a 'genuine' helix. This asymptotic formulation leads to finite expressions for the rod/matrix interaction. The helical-foundation is found in terms of finite helix-pitch-dependent, nonlinear parametric expressions. As a result, the problem is reduced to a system of finite nonlinear equations. This asymptote is shown to be valid for a rather large range of the helix angle.

## 2. Some preliminary remarks

We consider a right-hand rotation helical elastic rod embedded in a matrix. We denote the central curvilinear axis of the rod, as the $s$-axis, represented by a helix of radius $r_0$ (Fig. 1) and let the angle between the helix and its axis ($x$-axis; $x \equiv x_1$) be $\alpha_0$. In the following, we write *helix* to distinguish this central helix from others.

The *helix* can be characterized by the orthogonal Frenet triad $\boldsymbol{\tau}$, $\boldsymbol{n}$, $\boldsymbol{b}$:

$$\boldsymbol{\tau} = \mathbf{R}', \tag{1}$$

$$\boldsymbol{\tau}' = \kappa_0 \boldsymbol{n}, \quad \kappa_0 = \frac{\sin^2 \alpha_0}{r_0}, \tag{2}$$

$$\boldsymbol{n}' = -\kappa_0 \boldsymbol{\tau} + t_0 \boldsymbol{b}, \quad t_0 = \frac{\sin\ \alpha_0\ \cos\ \alpha_0}{r_0}, \tag{3}$$

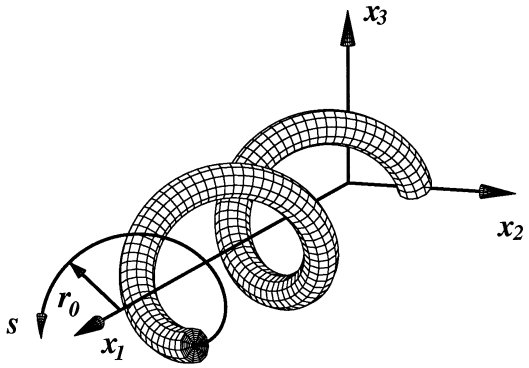


Fig. 1. The helical rod and the $X$-coordinate system.

$$\boldsymbol{b}' = -t_0\boldsymbol{n}, \quad l = 2\pi r_0 \cot \alpha_0, \tag{4}$$

where, here and below,

$$(\cdot)' = \frac{\mathrm{d}(\cdot)}{\mathrm{d}s},$$

and where $\boldsymbol{R}$ is the position vector; $\boldsymbol{\tau}$, $\boldsymbol{n}$ and $\boldsymbol{b}$ are the unit vectors (tangent, main normal and bi-normal, respectively); $\kappa_0$ is the curvature, $t_0$ is the torsion of the curve and $l$ is the pitch of the *helix*.

The geometric and material characteristics of the rod are assumed to be $s$-independent — in a *helix*-associated coordinate system — in accordance with the translation-rotation symmetry of the *helix*. In addition, the rod cross-section is taken as symmetric about the main normal to the *helix* thus leading to reflection symmetry.

Under these conditions, simple states of the composite are considered in which the components of tensors (in the description of the state) are $s$-independent as are the above-mentioned characteristics. Accordingly, uniform axial and radial extension of the composite and its torsion around the $x$-axis are considered.

Additional restrictions such as constitutive law, homogeneity, linearity, etc. are not introduced at this stage. However, we note here that the complete study of the problem is carried out below under a formulation where the geometrically nonlinear elastic rod is assumed to have a circular cross-section and the infinite matrix is considered in the framework of the linear elasticity. A circular cross-section is not only most natural for a fibre inclusion but also leads to a simplified determination of the rod/matrix interaction force and moment based on the stress field in the matrix.

## 3. Coordinate systems

We define a helical transformation as a rigid translation-rotation movement of a material space such that material points belonging to the *helix* (the curvilinear $s$-axis) and its axis (the $x$-axis) remain on the $s$- and $x$-axes, respectively. We seek a state which is invariant under this transformation. Our goal here is to construct a *helix*-related coordinate system such that only one coordinate, $s$, is variable under the helical transformation. Clearly, under these conditions, any point of the composite moves along some helix. Thus, we construct, by this definition, a family of coordinates which consists of coaxial helices having the same pitch and direction of rotation.

Let $r$ be the radius of any given helix of this family and let $\alpha$ be the angle between the helix and the $x$-axis (for the central *helix*, $r = r_0$, $\alpha = \alpha_0$). The rotation angle $\psi$ can then be expressed as

$$\psi = \frac{x \tan \alpha}{r} = \frac{x \tan \alpha_0}{r_0} \tag{5}$$

and hence,

$$\alpha(r) = \arctan\left(\frac{r}{r_0}\tan\ \alpha_0\right). \tag{6}$$

We now show that there exists no surface orthogonal to the first family, i.e. to the family of $s$-coordinates. Assume, for a moment, that such a surface, $S$, does exist. Its intersection with a cylindrical surface of radius $r$ is a curve, $\eta$, orthogonal to the helices lying on this cylindrical surface, and hence, it is also a helix (a 'conjugate' helix) which forms an angle $\alpha(r)-\pi/2$ with the axis. Furthermore, a straight radial line orthogonal to the axis must belong to $S$ since it is orthogonal to each helix (and conjugate helix) crossed. Consider a regular (non-singular) point on $S$. In a vicinity of this point, the surface (if it exists) can be represented as

$$x = x(r, \eta). \tag{7}$$

We then have

$$\frac{\partial x}{\partial \eta} = \sin\ \alpha, \quad \frac{\partial x}{\partial r} = 0$$

$$\frac{\partial}{\partial r}\ \frac{\partial x}{\partial \eta} = \frac{r_0^2\ \tan\ \alpha_0}{(r_0^2 + r^2\ \tan^2\ \alpha_0)^{3/2}} \neq \frac{\partial}{\partial \eta}\ \frac{\partial x}{\partial r} \equiv 0. \tag{8}$$

It follows from this inequality that the representation (7) does not exist and hence, such a surface does not exist; thus no global orthogonal coordinate system exists with the helices as a family of coordinate lines.

Therefore, among helix-associated coordinate systems only oblique-angled global systems are defined below. In addition, rectangular local coordinate systems are used. The following coordinate systems are defined:

$X$-system: a global rectangular Cartesian system $x_m$, $m = 1, 2, 3$; $x_1 \equiv x$ ($s = 0$ at $x = 0$, Fig. 1).

$C$-system: a cylindrical system, $x$, $r$, $\theta$ (Fig. 2a) related to the $X$-system such that the *helix* crosses the plane $x = 0$ at $r = x_2 = r_0$, $\theta = x_3 = 0$. In this system, the radial displacement is denoted by the subscript $r$. [This system is used to describe uniform strain of the matrix (in the absence of the rod).]

$H$-system: a local, rectangular Cartesian system $\xi_m$ with the origin at a point, $s$, of the *helix* (Fig. 2b). In this system, $\xi_1$ is parallel to $x$ ($\xi = x - s\cos\alpha_0$) and $\xi_3$ is directed toward the $x$-axis along the main normal to the *helix*. The $x$-axis crosses the $\xi_2$, $\xi_3$-plane at the point $(0, 0, r_0)$. Note that after displacements of the $X$-system ($s\cos\alpha_0$ and $r_0$, along $x_1$ and $x_2$, respectively), and its revolution about the *helix* axis by an angle $\pi/2 + \psi$, $\psi = s\sin\alpha_0/r_0$, the $X$-system coincides with the $H$-system. (The $H$-system is used for the representation of the fundamental fields produced by a concentrated force or a concentrated moment applied at the origin of the coordinate system in a space filled entirely by the matrix material.)

*T*-system: *s, n, b*, where, according to the Frenet triad, *n* and *b* are Cartesian rectangular coordinates in a plane orthogonal to the *helix* (Fig. 2c). A helical coordinate line, *s*, connects points with the same couple of *n, b*. The angle between *s* and this plane depends on the distance from the *helix* [at the *helix* it is $\pi/2$, see (6)]. In this system, the displacement directed toward the helix axis is denoted by the subscript *n*. Note that this displacement differs from that in the *C*-system by sign only. (This system is used in the formulation of the equilibrium equations of the helical rod.)

*TC*-system: *s,* $\rho$*,* $\phi$ with the locally cylindrical coordinates on the plane $s =$ const: $n=\rho\cos\phi$, $b=\rho\sin\phi$ (Fig. 2d). Relations between the coordinate systems are presented in the Appendix. (This system is used in calculating the rod/matrix interaction force and moment.)

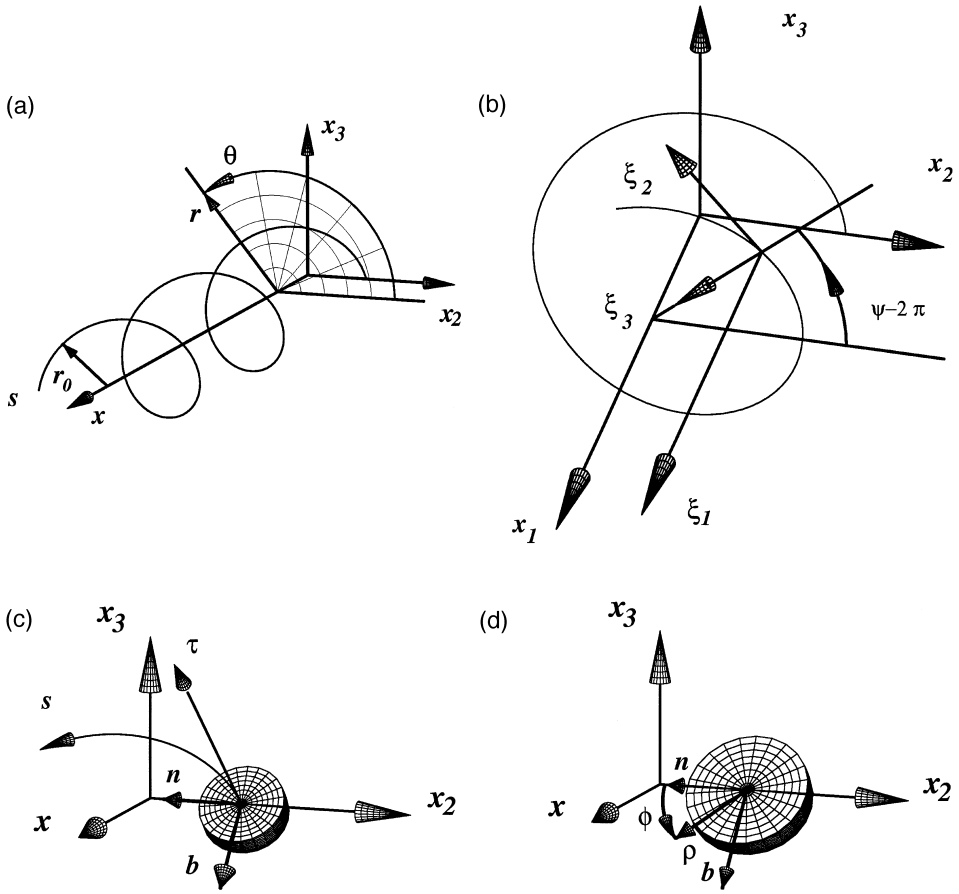


Fig. 2. (a) The helical rod axis and the cylindrical *C*-system. (b) The *H*-system. (c) The *T*-system. (d) The *TC*-system at $s = 0$.

Consider the oblique-angled helix-associated $T$- and $TC$-systems. The position vector can be represented as

$$\boldsymbol{R} = \boldsymbol{R}_a + n\boldsymbol{n} + b\boldsymbol{b} \tag{9}$$

where $\boldsymbol{R}_a$ corresponds to a point at the *helix*. From this, it follows that

$$\boldsymbol{R}' = (1 - \kappa_0 n)\boldsymbol{\tau} + t_0(n\boldsymbol{b} - b\boldsymbol{n}) = (1 - \kappa_0 n)\boldsymbol{\tau} + t_0\rho\boldsymbol{k}_\phi, \tag{10}$$

where $\boldsymbol{k}_\phi$ is the tangent unit vector (Fig. 3).

Thus, the vector $\boldsymbol{R}'$ contains a rotational component proportional to the distance, $\rho$, from the $n$, $b$-origin. Note that this coordinate system can be obtained by the corresponding bending and torsion of a rectangular Cartesian system initially associated with a straight line. The length of the tangent vector, $\boldsymbol{R}'$, is

$$H_1 = |\boldsymbol{R}'| = \sqrt{(1 - \kappa_0 n)^2 + t_0^2\rho^2}, \tag{11}$$

where $\rho^2 = n^2 + b^2$.

In the following, we assume the rod to be of circular cross-section, $0 \le \rho \le \rho_0$. Note that the expression (11) can be simplified if the curvature of the *helix* is small and the angle $\alpha_0$ is not too close to $\pi/2$, namely if

$$\kappa_0\rho_0 \ll \cos\ \alpha_0. \tag{12}$$

In this case, for $\rho \le \rho_0$, this length,

$$H_1 = |\boldsymbol{R}'| \sim \sqrt{1 + t_0^2\rho^2}, \tag{13}$$

can be considered as $\phi$-independent.

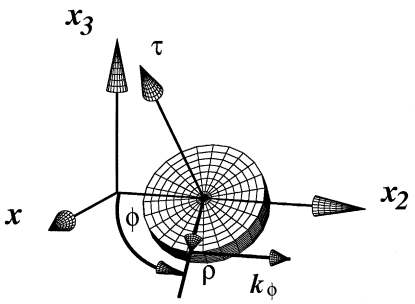


Fig. 3. The tangent unit vector.

## 4. Equilibrium of the helical rod

The orthogonal triad $\boldsymbol{\tau}$, $\boldsymbol{n}$, $\boldsymbol{b}$ natural to the *helix* and the $T$-system are assumed to be associated with the actual state of the deformed rod.

The equilibrium equations for the rod are then as follows:

$$\boldsymbol{Q}' + \boldsymbol{q} = 0, \tag{14}$$

$$\boldsymbol{M}' + \boldsymbol{\tau} \times \boldsymbol{Q} + \mu = 0, \tag{15}$$

where the internal force acting on the rod's cross-section with the external normal $\boldsymbol{\tau}$ is

$$\boldsymbol{Q} = T\boldsymbol{\tau} + N\boldsymbol{n} + B\boldsymbol{b} \tag{16}$$

and the internal moment acting on the same cross-section is

$$\boldsymbol{M} = M_\tau \boldsymbol{\tau} + M_n \boldsymbol{n} + M_b \boldsymbol{b}. \tag{17}$$

The external force and moment distributed along the *helix* are accordingly

$$\boldsymbol{q} = q_\tau \boldsymbol{\tau} + q_n \boldsymbol{n} + q_b \boldsymbol{b},$$

$$\boldsymbol{\mu} = \mu_\tau \boldsymbol{\tau} + \mu_n \boldsymbol{n} + \mu_b \boldsymbol{b}. \tag{18}$$

For a simple state of the rod with $s$-independent components of the internal forces and moments, the equilibrium equations take the form

$$\kappa_0 N = q_\tau,$$

$$\kappa_0 T - t_0 B = -q_n,$$

$$t_0 N = -q_b,$$

$$\kappa_0 M_n = \mu_\tau,$$

$$\kappa_0 M_\tau - t_0 M_b - B = -\mu_n,$$

$$t_0 M_n + N = -\mu_b. \tag{19}$$

In particular, from this and from Eqs. (2) and (3) it follows that

$$q_x = q_\tau \cos \alpha_0 + q_b \sin \alpha_0 = 0,$$

$$q_\theta = q_\tau \sin \alpha_0 - q_b \cos \alpha_0 = \frac{\sin \alpha_0}{r_0} N,$$

$$\mu_x = \mu_\tau \cos \alpha_0 + \mu_b \sin \alpha_0 = -N \cos \alpha_0 = -q_\theta r_0,$$

$$\mu_\theta = \mu_\tau \sin \alpha_0 - \mu_b \cos \alpha_0 = \frac{\sin \alpha_0}{r_0} M_n + N \cos \alpha_0. \tag{20}$$

Eqs. (19) can then be rewritten in the following form:

$$\kappa_0 T - t_0 B = -q_n, \tag{21}$$

$$N = \frac{r_0}{\sin \alpha_0} q_\theta, \tag{22}$$

$$\kappa_0 M_\tau - t_0 M_b - B = -\mu_n, \tag{23}$$

$$M_n = \frac{r_0}{\sin \alpha_0} (\mu_\theta - q_\theta r_0 \cot \alpha_0), \tag{24}$$

$$q_x = 0, \tag{25}$$

$$\mu_x = -q_\theta r_0. \tag{26}$$

The number of unknowns can be essentially reduced by taking into account reflection symmetry, that is, equivalence of the 'forward' and 'back' directions along the $x$-axis. As was mentioned, this equivalence takes place if the cross-section of the rod possesses symmetry about the main normal, that is, with respect to the $b$-to-$(-b)$-transformation. Hence each component of any physical external vector must be invariant with respect to the transformation $(x, \theta)$ to $(-x, -\theta)$.

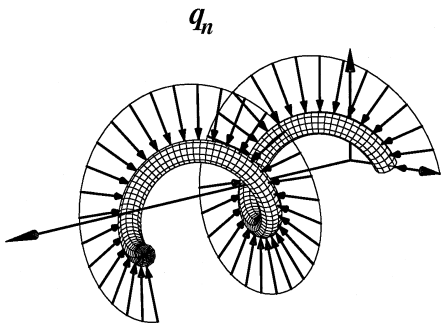


Fig. 4. The normal rod–matrix interaction force $q_n$ (the vector representation of the interaction moment $\mu_n$ has the same orientation).

From this, it follows that only normal-oriented vectors can exist (Fig. 4) and

$$q_\tau = q_b = \mu_\tau = \mu_b = 0. \tag{27}$$

Therefore, $N = M_n = 0$, and only two nontrivial equilibrium equations remain, namely

$$\kappa_0 T - t_0 B = -q_n, \tag{28}$$

$$\kappa_0 M_\tau - t_0 M_b - B = -\mu_n. \tag{29}$$

Consider an element of the rod bounded by two cross-sections with coordinates $s$ and $s + \mathrm{d}s$. Beside the external force, $q_n\,\mathrm{d}s$, and moment, $\mu_n\,\mathrm{d}s$, self-equilibrated tractions can act on the external surface of the element. Although such tractions can be present in the formulation of the problem using a higher-order rod model, for the case of a Bernoulli–Euler rod only non-self-equilibrated loads are significant. In the following, the latter model is used assuming the rod material to be sufficiently rigid in comparison with the matrix material.

## 5. Deformation of the rod and internal forces and moments

The deformation of the rod can be considered as consisting of an axis-associated deformation and internal torsion. The former state of a thin rod, its stretch, curvature and torsion, is defined as the state of its axis. Such is the case if, during deformation, the normal to the axis consists of the same material points. This means that the family of helices in the $T$-system represents material helices. The internal torsion corresponds to torsion of the rod such that its shape remains constant, namely that of the 'rigid' *helix*. Under internal torsion, material helices rotate about the coordinate helices. Internal torsion is not considered here.

We now express the initial parameters of the *helix* and the axis-associated deformation of the rod in terms of strain of the cylinder $0 \le r \le r_0$ (Fig. 5):

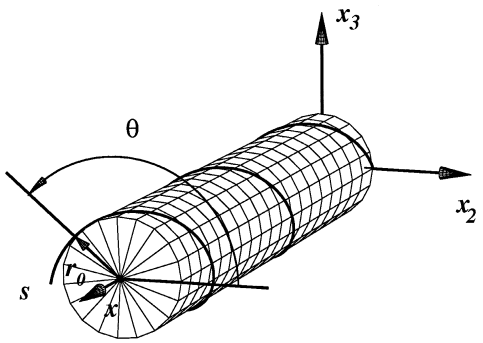


Fig. 5. The reference cylinder $r \le r_0$.

$$\lambda_x = \frac{\mathrm{d}x}{\mathrm{d}x^i}, \quad \lambda_r = \frac{r_0}{r_0^i}, \quad \gamma. \tag{30}$$

In the above, $x^i$ and $r_0^i$ are initial values of the material coordinate and *helix* radius, respectively, $\gamma$ is the torsion of the cylinder, i.e. the increase of the angle of revolution about the $x$-axis per unit length in the deformed state; $\lambda_x$ and $\lambda_r$ are corresponding stretches in the $x$- and $r$-directions, respectively. Recalling that $x = s \cos \alpha_0$, the stretch of the *helix* can be expressed as

$$\lambda_s = \frac{\mathrm{d}s}{\mathrm{d}s^i} = \frac{\cos\ \alpha_0^i}{\cos\ \alpha_0}\lambda_x. \tag{31}$$

Letting $(x, \theta)$ and $(x^i, \theta^i)$ be the $C$-coordinates of a material point of the *helix* in the deformed state and the initial state, respectively (at the origin of the coordinate system, $x = x^i = 0$), the following equalities then hold:

$$\theta = \frac{x\ \tan\ \alpha_0}{r_0},$$

$$\theta^i = \theta - x\gamma = \frac{x^i\ \tan\ \alpha_0^i}{r_0^i}. \tag{32}$$

It follows that

$$\tan\ \alpha_0^i = \frac{\lambda_x}{\lambda_r}(\tan\ \alpha_0 - \gamma r_0). \tag{33}$$

This formula defines the initial angle, $\alpha_0^i$ ($0 \le \alpha_0^i < \pi/2$). Now the *helix* stretch is determined by expression (31) and its initial curvature and torsion, namely by the corresponding expressions (2) and (3) now used for the values $r_0^i$, $\alpha_0^i$. Under condition (12), the axis-associated deformation of the rod, the longitudinal strain and variation of curvature and torsion, are defined by the corresponding parameters for the *helix* as determined above. Note that under the present considerations, lateral shear of the rod is neglected and hence, the material *helix* is normal to the material cross-sections in both the deformed and initial states of the rod. Further, the rotation of a rod cross-section about the $n$-axis can then be expressed as

$$\Theta = \Theta_n = \alpha_0 - \alpha_0^i. \tag{34}$$

Eqs. (30)–(34) yield the following representation, respectively, for the angle of rotation of the cross-section of the rod, the change of its curvature, $H$-torsion and the stretch of the rod:

$$\alpha_0 - \alpha_0^i = \arctan\left[\frac{(\lambda_r - \lambda_x)\tan\ \alpha_0 + \lambda_x\gamma r_0}{\lambda_r + \lambda_x(\tan\ \alpha_0 - \gamma r_0)\tan\ \alpha_0}\right], \tag{35}$$

$$\kappa_0 - \kappa_0^i = \kappa_0 \left[ 1 - \lambda_r \frac{(\tan\ \Theta - \tan\ \alpha_0)^2}{(1 + \tan^2 \Theta) \tan^2 \alpha_0} \right], \tag{36}$$

$$t_0 - t_0^i = t_0 \left[ 1 - \lambda_r \frac{\tan\ \alpha_0 (1 - \tan^2 \Theta) - \tan\ \Theta (1 - \tan^2 \alpha_0)}{(1 + \tan^2 \Theta) \tan\ \alpha_0} \right], \tag{37}$$

$$\lambda_s = \lambda_x \frac{1 + \tan\ \alpha_0\ \tan\ \Theta}{\sqrt{1 + \tan^2 \Theta}}. \tag{38}$$

For the cylinder $r = r_0$ undergoing small strains, i.e. when $(\epsilon_x, \epsilon_r, \gamma) \ll 1$, the above relations take the form

$$\Theta \sim (\epsilon_r - \epsilon_x) \sin\ \alpha_0\ \cos\ \alpha_0 + \gamma r_0\ \cos^2 \alpha_0, \quad \epsilon_x = \lambda_x - 1, \quad \epsilon_r = \lambda_r - 1, \tag{39}$$

$$\kappa_0 - \kappa_0^i \sim 2 t_0 \Theta - \kappa_0 \epsilon_r, \tag{40}$$

$$t_0 - t_0^i \sim k_0 \Theta \frac{1 - \tan^2 \alpha_0}{\tan^2 \alpha_0} - t_0 \epsilon_r, \tag{41}$$

$$\epsilon_s = \lambda_s - 1 \sim \Theta\ \tan\ \alpha_0 + \epsilon_x. \tag{42}$$

Assuming the rod material to be elastic and the linear Hook's law to be valid, we can express the internal longitudinal force and moment as follows:

$$T = EA(\lambda_s - 1), \tag{43}$$

where $E$ is the Young elastic modulus of the rod material, and $A$ is the cross-section area,

$$M_b = EI(\kappa_0 - \kappa_0^i) \tag{44}$$

and where $I$ is the moment of inertia (for the homogeneous circular cross-section, $I = \pi \rho_0^4/4$). The torsional moment is expressed as

$$M_\tau = GI_p(t_0 - t_0^i), \tag{45}$$

where $G$ is the shear modulus of the rod material and $I_p$ is the polar moment of inertia (for the homogeneous circular cross-section $I_p = \pi \rho_0^4/2$).

Note that the shear force $B$ is not determined here from the shear strain since the latter is neglected. Instead we assume the perpendicularity condition for the *helix* and the rod cross-section.

Note that strain of the *helix* can be small, $|\lambda_s - 1| \ll 1$, even under a large deformation. In this case, the dependence of $\lambda_r$ on $\lambda_x$ becomes $\lambda_s$-dependent:

$$\lambda_r = \lambda_x \frac{\tan\ \alpha_0 - \gamma r_0}{\sqrt{(\lambda_x/\lambda_s\ \cos\ \alpha_0)^2 - 1}} \sim \lambda_x \frac{\tan\ \alpha_0 - \gamma r_0}{\sqrt{(\lambda_x/\cos\ \alpha_0)^2 - 1}}. \tag{46}$$

By way of example, let us consider a limiting deformation of an inextensible *helix* which degenerates to a straight line. Let $\gamma = \gamma_0 = 0$. In this case, the stretch $\lambda_x = 1/\cos\ \alpha_0^i \lambda_s = 1$. Under this deformation

$$\theta = \frac{x\ \tan\ \alpha_0}{r_0} \quad \text{and} \quad s = \frac{x}{\cos\ \alpha_0} \tag{47}$$

are invariable and hence,

$$t_0 = \frac{\sin\ \alpha_0^i}{r_0^i}. \tag{48}$$

This relation shows how the rotation of the *helix* and hence, *H*-torsion of the helical bar vary when the *helix* is strained [1].

## 6. Kelvin's fundamental solutions

We seek the response of the matrix surrounding the rod to the action of a force, $q_3 = -q_n$, and moment, $\mu_3 = -\mu_n$ uniformly distributed along the bar (Fig. 4). Using the *H*-system, we note that the subscript '3' denotes the corresponding component in this system, while $q_n$ (28) and $\mu_n$ (29) are the force and the moment acting on the rod. Also note that in this context, 'uniformly' means that these components applied to the matrix by the rod are *s*-independent. Thus, the problem here concerns the external domain surrounding the helical rod.

We obtain a solution according to the following procedure. The displacement and stress fields produced by a concentrated force in an unbounded elastic space (in the absence of the rod) are first determined using Kelvin's fundamental solution. The corresponding fields due to a concentrated moment can then be easily obtained. Superposition of the fields induced by such forces and moments directed toward the *helix* axis and uniformly distributed along the *helix* represents the required fields. In this way, the rod/matrix interaction force is represented as a sum of two terms: the first is proportional to the force distributed along the *helix* and the second is proportional to the moment also distributed along the *helix*. A similar representation is used for the rod/matrix interaction moment.

In this formulation, the stress field is constructed to correspond to arbitrary values of the force and the moment, which are then determined uniquely. In doing so, the stress field is uniquely determined as well. However, this uniqueness is a consequence of the formulation, where only singularities corresponding to the force and moment are distributed along the rod axis. In fact, an additional self-

[1] Large torsion under such elongation explains why a cable reeled out from a coil must be untwisted.

equilibrated part of the field (self-equilibrated at the rod cross-section boundary) must be present in the exact solution. However, it cannot be found based on the formulation adopted above since the corresponding interface conditions are not taken into account. This additional field can have an importance in itself, especially for the determination of the initiation of delamination and fracture of the matrix. Moreover, the solution with a 'correct' self-equilibrated field may correspond to a corrected non-self-equilibrated force/moment field as well.

The rough approximation used in this study is justified since it yields reasonable results in the homogenization. Note that the self-equilibrated fields are local, near-rod fields, and the geometric nonlinearity concerns them as well as the rod. In the approach to the problem which is adopted, the nonlinearity in the description of the low-modulus matrix is neglected assuming it to be a 'second-order' effect. This approach seems to be reasonable for the determination of the deformation of the rod and for an estimation of the effective properties of the composite. The problem for the local, near-rod fields, which are important mainly for the estimation of fracture initiation, is still open. At the same time, the field induced by the distributed force/moment singularities creates a framework for the local field representing conditions far from the bar. In addition, this non-self-equilibrated field solution yields an estimate of the effective region of the complete field location since the self-equilibrated components decay with the distance from the rod faster than the former components.

Thus, the concentrated forces and moments play an auxiliary role, as they remain outside the real domain of the matrix. The unknown force and moment densities are then determined using the condition of continuity of the displacement and rotation at the interface $\rho = \rho_0$. However, in this section, only the fields produced by unit concentrated forces and moments are considered.

Consider a space filled entirely by the matrix material. Although the helical rod is not considered to be present, we express the required quantities in terms of the above introduced $H$-system, Fig. 2b. We consider the space to be subjected to the concentrated force, $q_h^0$, and moment, $\mu_h^0$, applied at the origin of the $H$-system at a point $s$ and directed along the $h$-axis ($h = 1, 2, 3$). Let ${}^q u_m^h(\xi_1, \xi_2, \xi_3)$ and ${}^\mu u_m^h(\xi_1, \xi_2, \xi_3)$, $m = 1, 2, 3$, be the $m$-components of displacements induced by the unit force ($q_h^0 = 1$) and moment ($\mu_h^0 = 1$), respectively. The left superscripts used for the fundamental stresses, ${}^q\sigma_{ml}^h$ and ${}^\mu\sigma_{ml}^h$, have the same sense ($m, l = 1, 2, 3$). The components of displacements follow from the general Papkovich–Neuber representation (see, e.g., Fung, 1965)

$$ {}^q u_m = 4(1-\nu)\Phi_m - \frac{\partial}{\partial \xi_m} \sum_{l=0}^{3} \xi_l \Phi_l, \quad \xi_0 = 1. \tag{49} $$

For the case considered,

$$ \Phi_l = \frac{1+\nu}{8\pi(1-\nu)E_M R}\delta_{lh}, \quad R^2 = \sum_{m=1}^{3} \xi_m^2, \tag{50} $$

where $\nu$ is the Poisson's ratio, $E_M$ is the Young modulus of the matrix and $\delta_{lh}$ is the Kronecker delta. Therefore, we have

$$ {}^{q}u_m^h = \frac{1+\nu}{8\pi(1-\nu)E_M}\left(\frac{\xi_m\xi_h}{R^3} + (3-4\nu)\frac{\delta_{mh}}{R}\right). \tag{51} $$

The stress components are expressed as follows:

$$ {}^{q}\sigma_{ml}^h = \frac{1}{8\pi(1-\nu)}\left[(1-2\nu)\frac{\xi_h\delta_{ml} - \xi_m\delta_{lh} - \xi_l\delta_{mh}}{R^3} - \frac{3\xi_m\xi_l\xi_j}{R^5}\right]. \tag{52} $$

Displacements induced by the unit moment $\mu_3^0 = 1$ are [2]

$$ {}^{\mu}u_m^3 = \frac{1}{2}\left(\frac{\partial {}^{q}u_m^1}{\partial\xi_2} - \frac{\partial {}^{q}u_m^2}{\partial\xi_1}\right) = \frac{1+\nu}{4\pi E_M}\,\frac{\xi_1\delta_{m2} - \xi_2\delta_{m1}}{R^3}. \tag{53} $$

The corresponding stress components are given as

$$ {}^{\mu}\sigma_{ml}^3 = \frac{1}{2}\left(\frac{\partial {}^{q}\sigma_{ml}^1}{\partial\xi_2} - \frac{\partial {}^{q}\sigma_{ml}^2}{\partial\xi_1}\right) = \frac{3}{8\pi}\,\frac{\xi_2(\xi_m\delta_{l1} + \xi_l\delta_{m1}) - \xi_1(\xi_m\delta_{l2} + \xi_l\delta_{m2})}{R^5}. \tag{54} $$

Note that displacements and stresses corresponding to moments $\mu_1^0$ and $\mu_2^0$ can be obtained from the expressions (53) and (54) by means of the cyclic permutation of the explicitly written indices.

Thus, the displacement components induced by the unit force and moment directed towards the helix axis ($h = 3$) are

$$ {}^{q}u_1^3 = \frac{1+\nu}{8\pi(1-\nu)E_M}\,\frac{\xi_1\xi_3}{R^3}, \quad {}^{q}u_2^3 = \frac{1+\nu}{8\pi(1-\nu)E_M}\,\frac{\xi_2\xi_3}{R^3}, $$

$$ {}^{q}u_3^3 = \frac{1+\nu}{8\pi(1-\nu)E_M}\left(\frac{\xi_3^2}{R^3} + \frac{3-4\nu}{R}\right) $$

$$ {}^{\mu}u_1^3 = -\frac{1+\nu}{4\pi E_M}\,\frac{\xi_2}{R^3}, \quad {}^{\mu}u_2^3 = \frac{1+\nu}{4\pi E_M}\,\frac{\xi_1}{R^3}, \quad {}^{\mu}u_3^3 = 0. \tag{55} $$

Finally, the stress components are written as

$$ {}^{q}\sigma_{11}^3 = \frac{1}{8\pi(1-\nu)}\left[\frac{(1-2\nu)\xi_3}{R^3} - \frac{3\xi_1^2\xi_3}{R^5}\right], $$

[2] A pure moment without shear singularity is considered because lateral shear of the bar is neglected.

$$
{}^{q}\sigma_{22}^{3} = \frac{1}{8\pi(1-\nu)}\left[\frac{(1-2\nu)\xi_3}{R^3} - \frac{3\xi_2^2\xi_3}{R^5}\right],
$$

$$
{}^{q}\sigma_{33}^{3} = -\frac{1}{8\pi(1-\nu)}\left[\frac{(1-2\nu)\xi_3}{R^3} + \frac{3\xi_3^3}{R^5}\right],
$$

$$
{}^{q}\sigma_{12}^{3} = -\frac{3}{8\pi(1-\nu)}\,\frac{\xi_1\xi_2\xi_3}{R^5},
$$

$$
{}^{q}\sigma_{13}^{3} = -\frac{1}{8\pi(1-\nu)}\left[\frac{(1-2\nu)\xi_1}{R^3} + \frac{3\xi_1\xi_3^2}{R^5}\right],
$$

$$
{}^{q}\sigma_{23}^{3} = -\frac{1}{8\pi(1-\nu)}\left[\frac{(1-2\nu)\xi_2}{R^3} + \frac{3\xi_2\xi_3^2}{R^5}\right],
$$

$$
{}^{\mu}\sigma_{11}^{3} = \frac{3}{4\pi}\,\frac{\xi_1\xi_2}{R^5}, \quad {}^{\mu}\sigma_{22}^{3} = -{}^{\mu}\sigma_{11}^{3}, \quad {}^{\mu}\sigma_{33}^{3} = 0,
$$

$$
{}^{\mu}\sigma_{12}^{3} = \frac{3}{8\pi}\,\frac{\xi_2^2-\xi_1^2}{R^5}, \quad {}^{\mu}\sigma_{13}^{3} = \frac{3}{8\pi}\,\frac{\xi_2\xi_3}{R^5}, \quad {}^{\mu}\sigma_{23}^{3} = -\frac{3}{8\pi}\,\frac{\xi_1\xi_3}{R^5}. \tag{56}
$$

## 7. Fields in the matrix at the interface

We now use the $T$-system in which we must find the force, $q_n$, and moment, $\mu_n$, acting on the prospective cross-section of the rod, as well as its displacement, $U_n$ and rotation, $\Theta_n$. (As was mentioned above, since it follows from the symmetry of the problem that all vectors are oriented along the main normal to the *helix*, that is, in the $T$-system, only components with the subscript $n$ remain.)

A two-dimensional element of the interface is formed by a one-dimensional element of the cross-section boundary and the one-dimensional element which is normal to the cross-section [see the first term in the expression of $\boldsymbol{R}'$ (10)]. According to the accuracy as defined in (12), this component is the unit tangent vector. Hence, the radial displacement of the rod, the force and the moment can be found in terms of displacements and stresses, properly averaged over the circumference $\rho = \rho_0$. With this in mind, we define the following components of displacements and stresses along this circumference (Fig. 6):

$u_1^0 \equiv u_\tau(0, \rho_0, \phi)$ – the displacement in $\boldsymbol{\tau}$-direction,

$u_2^0 \equiv u_n(0, \rho_0, \phi)$ – the displacement in $\boldsymbol{n}$-direction,

$$\sigma^0_{22} \equiv \sigma_{nm}(0, \rho_0, \phi) \quad \text{and} \quad \sigma^0_{32} \equiv \sigma_{bn}(0, \rho_0, \phi) \; - \text{ the stresses acting in } \boldsymbol{n}\text{-direction},$$

$$\sigma^0_{21} \equiv \sigma_{n\tau}(0, \rho_0, \phi) \quad \text{and} \quad \sigma^0_{31} \equiv \sigma_{b\tau}(0, \rho_0, \phi) \; - \text{ the stresses acting in } \boldsymbol{\tau}\text{-direction}. \tag{57}$$

These components, expressed in terms of the fundamental solutions, are

$$u^0_m = \gamma_{ml}[q^0_3 q u^3_l(\xi_1, \xi_2, \xi_3) + \mu^0_3 \mu u^3_l(\xi_1, \xi_2, \xi_3)],$$

$$\sigma^0_{ml} = \gamma_{mp}\gamma_{lq}[q^0_3 q \sigma^3_{pq}(\xi_1, \xi_2, \xi_3) + \mu^0_3 \mu \sigma^3_{pq}(\xi_1, \xi_2, \xi_3)], \tag{58}$$

where $q^0_3$ and $\mu^0_3$ are the unknown force and moment distributed along the *helix*. The displacements and stresses on the right-hand-side are defined in the $H$-system [see (55) and (56)]; coordinates $\xi_m$ and the spin matrix $C \equiv [\gamma_{ml}]$ are presented in the Appendix.

The values averaged over the cross-section boundary have the following expressions:

$$U^0_n = -U^0_r = \frac{1}{2\pi}\int_0^{2\pi} u^0_2 \, \mathrm{d}\phi, \tag{59}$$

$$\Theta^0_n = \frac{1}{\pi\rho_0}\int_0^{2\pi} u^0_1 \, \sin\, \phi \, \mathrm{d}\phi, \tag{60}$$

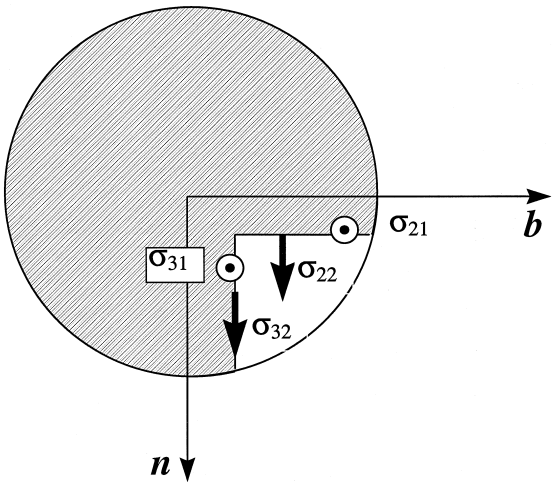


Fig. 6. Components of stresses at the rod–matrix interface.

$$q_n^0 = q_2^0 = \rho_0 \int_0^{2\pi} (\sigma_{22}^0 \cos\ \phi + \sigma_{32}^0 \sin\ \phi) \mathrm{d}\phi, \tag{61}$$

$$\mu_n^0 = \mu_2^0 = -\frac{1}{2}\rho_0^2 \int_0^{2\pi} [\sigma_{21}^0 \sin\ 2\phi + \sigma_{31}^0 (1 - \cos\ 2\phi)] \mathrm{d}\phi. \tag{62}$$

Here $U_r^0 = r_0 - r_0^i$ is the displacement of the matrix with positive direction along the $r$-axis in the $C$-system.

We now consider the matrix under such a loading (body force and moment), uniformly distributed along the *helix* and let $q_3^0$ and $\mu_3^0$ (independent of $s$) be the corresponding distributions per unit length of the *helix*. In this case, the fields can be found by our superposition. For example,

$$U_r =^q U_r q_3^0 +^\mu U_r \mu_3^0 = \int_{-\infty}^{\infty} U_r^0 \, \mathrm{d}s, \quad \Theta_n =^q \Theta_r q_3^0 +^\mu \Theta_r \mu_3^0 = \int_{-\infty}^{\infty} \Theta_n^0 \, \mathrm{d}s, \tag{63}$$

$$q_n =^q q_n q_3^0 +^\mu q_n \mu_3^0 = \int_{-\infty}^{\infty} q_n^0 \, \mathrm{d}s, \quad \mu_n =^q \mu_n q_3^0 +^\mu \mu_n \mu_3^0 = \int_{-\infty}^{\infty} \mu_n^0 \, \mathrm{d}s. \tag{64}$$

In relations (63) and (64), the left superscripts $q$ and $\mu$ correspond to the assumptions $\mu_3^0 = 0$ and $q_3^0 = 0$, respectively, the same as in the previous section. Due to symmetry the components obtained are $s$-independent.

## 8. System of equations with respect to unknown forces

When the $s$-independent components of the displacement and the angle of rotation of the cross-section of the rod as well as distributed forces and moments acting on the *helix* are calculated [see Eqs. (63)], the unknown force $q_3^0$ and moment $\mu_3^0$ can be found using equilibrium equations for the rod, Eqs. (28), (29) and compatibility conditions. These calculations are performed in terms of given axial, $\lambda_x$, and radial, ${}^\infty\lambda_r$, stretches and torsion $\gamma$, of the cylinder $0 \le r \le r_0$, Eq. (30).

The total radial displacement of the matrix averaged over the cross-section boundary of the rod is expressed below as a sum of three terms. The first, ${}^\infty U_r = r_0({}^\infty\lambda_r - 1)$, is the free-rod displacement of the matrix at $r = r_0$ (in the $C$-system) which corresponds to the given uniform radial strain of the matrix (without any influence of the rod). The second corresponds to the rod/matrix interaction force, and the third, to the interaction moment. Thus, the total displacement is as follows (positive displacements $U$ and $U_r$ are directed away from the $x$-axis of the helix):

$$U =^0 U_r +^q U_r q_3^0 +^\mu U_r \mu_3^0. \tag{65}$$

Using this and the equivalence of radial displacements of the matrix and of the

rod,

$$U = r_0 - r_0^i, \tag{66}$$

we obtain the initial radius of the *helix* and the radial stretch, $\lambda_r$, of the cylinder considered, in terms of $q_3^0$ and $\mu_3^0$:

$$r_0^i = \frac{1}{{}^{\infty}\lambda_r}(r_0 - {}^{q}U_r q_3^0 - {}^{\mu}U_r \mu_3^0) \tag{67}$$

$$\lambda_r = \frac{r_0}{r_0^i} = \frac{{}^{\infty}\lambda_r r_0}{r_0 - {}^{q}U_r q_3^0 - {}^{\mu}U_r \mu_3^0}. \tag{68}$$

Finally, the second compatibility condition $\Theta_{in}^0 = \Theta = \alpha_0 - \alpha_0^i$ combined with the equations of the equilibrium of the rod, Eqs. (28) and (29), leads to the system of three nonlinear algebraic equations with respect to $q_3^0$, $\mu_3^0$ and shear force, $B$. We present here this system and all additional equations explicitly.

### 8.1. The system of equations with respect to $q_3^0$, $\mu_3^0$ and $B$

$$\alpha_0 - \alpha_0^i = {}^{q}\Theta_n q_3^0 + {}^{\mu}\Theta_n \mu_3^0, \tag{69}$$

$$\kappa_0 T - t_0 B = -q_n = -({}^{q}q_n q_3^0 + {}^{\mu}q_n \mu_3^0), \tag{70}$$

$$\kappa_0 M_\tau - t_0 M_b - B = -\mu_n = -({}^{q}\mu_n q_3^0 + {}^{\mu}\mu_n \mu_3^0). \tag{71}$$

Here the values $\Theta_n$, $q_n$ and $\mu_n$ are functions of unknown distributions $q_3^0$ and $\mu_3^0$ and are calculated using Eqs. (63) and (64). Note that in the case of a sliding rod/matrix contact, the equation $\mu_n = 0$ must be used instead of Eq. (69).

### 8.2. The change of angle of rotation, curvature, torsion and stretch of the rod as functions of the stretches of the cylinder $0 \le r \le r_0$

$$\alpha_0 - \alpha_0^i = \arctan\left[\frac{(\lambda_r - \lambda_x)\tan\ \alpha_0 + \lambda_x \gamma r_0}{\lambda_r + \lambda_x(\tan\ \alpha_0 - \gamma r_0)\tan\ \alpha_0}\right], \tag{72}$$

$$\kappa_0 - \kappa_0^i = \kappa_0\left[1 - \lambda_r \frac{(\tan\ \Theta - \tan\ \alpha_0)^2}{(1 + \tan^2 \Theta)\tan^2 \alpha_0}\right], \tag{73}$$

$$t_0 - t_0^i = t_0\left[1 - \lambda_r \frac{\tan\ \alpha_0(1-\tan^2\ \Theta) - \tan\ \Theta(1-\tan^2\ \alpha_0)}{(1+\tan^2\ \Theta)\tan\ \alpha_0}\right], \tag{74}$$

$$\lambda_s = \lambda_x \frac{1+\tan\ \alpha_0\ \tan\ \Theta}{\sqrt{1+\tan^2\ \Theta}}. \tag{75}$$

Linearized equations for small strains are presented in Eqs. (39)–(41).

*8.3. Internal forces and moments within the rod as functions of stretches, curvatures and torsion*

$$T = EA(\lambda_s - 1), \tag{76}$$

$$M_b = (\kappa_0 - \kappa_0^i)EI, \tag{77}$$

$$M_\tau = GI_p(t_0 - t_0^i). \tag{78}$$

Note that for small strains of the cylinder, $r = r_0$, the linearized equations (39)–(41) are used. In this case Eqs. (69)–(71) become quadratic with respect to $q_3^0$, $\mu_3^0$. If, additionally, $r_0 \neq 0$ and the radial displacement caused by forces and moments acting on the rod is small in comparison with the radius of the cylinder $U_r \ll r_0$, the radial stretch can be represented as follows

$$\lambda_r \sim {}^{\infty}\lambda_r\left[1 + \frac{{}^{q}U_r}{r_0}q_3^0 + \frac{{}^{\mu}U_r}{r_0}\mu_3^0\right]. \tag{79}$$

In this case the system of equations becomes linear and can be solved explicitly.

When (for given $\lambda_r$, $\lambda_x$ and $\gamma$) $q_3^0$, $\mu_3^0$ and $B$ are found, internal forces and moments within the rod as well as its deformations can be calculated by backward substitution using Eqs. (72)–(78).

## 9. Asymptotic relations based on the condition (12)

The fundamental solutions contained in the superposition integrals (63) and (64) depend, in particular, on the distance, $R$, between the external concentrated force/moment application point and the point considered. It follows from (A6) that

$$R^2 = 2r_0^2(1-\cos\ \psi) + s^2\ \cos^2\ \alpha + \rho_0^2 - 2r_0\rho_0[\cos\ \alpha(\psi - \sin\ \psi)\sin\ \phi + (1-\cos\ \psi)\cos\ \phi]. \tag{80}$$

Using condition (12), we now show that the last term (contained in square

brackets) of expression (80) is relatively small. Indeed, all the terms in the first line in (80) are non-negative and two strong inequalities are valid:

$$\frac{2r_0\rho_0\ \cos\ \alpha(\psi-\sin\ \psi)\sin\ \phi}{s^2\ \cos^2\alpha} = \frac{2(\psi-\sin\ \psi)\sin\ \phi}{\psi^2}\ \frac{\kappa\rho_0}{\cos\ \alpha} \le \frac{2}{\pi}\ \frac{\kappa\rho_0}{\pi\ \cos\ \alpha} \ll 1 \tag{81}$$

and

$$\frac{2r_0\rho_0\ \cos\ \alpha(1-\cos\ \psi)\cos\ \phi}{s^2\ \cos^2\alpha + 2r_0^2(1-\cos\ \psi)} = \frac{2\kappa\rho_0\ \cos\ \phi(1-\cos\ \psi)}{2\ \sin^2\alpha(1-\cos\ \psi-\psi^2/2)+\psi^2} \le \kappa\rho_0 \ll 1. \tag{82}$$

Thus, under the condition (12), the distance can be assumed to be $\phi$-independent, i.e.

$$R^2 = 2r_0^2(1-\cos\ \psi) + s^2\ \cos^2\alpha + \rho_0^2. \tag{83}$$

This simplifies considerably the determination of the values averaged over the circumference $\rho=\rho_0$. The integrals in the expressions (59)–(62) can now be calculated explicitly. As a result, we obtain:

$$U_n^0 =^q U_n^0 q_3^0 +^\mu U_n^0 \mu_3^0,$$

$$^qU_n^0 = \frac{1+\nu}{16\pi E_M(1-\nu)R}\left[2(4\nu-3)\cos\ \psi + \frac{2r_0^2(1-\cos\ \psi)^2-\rho_0^2\ \cos\ \psi}{R^2}\right],$$

$$^\mu U_n^0 = \frac{(1+\nu)r_0\psi\ \sin\ \psi\ \cos\ \alpha_0}{4\pi E_M\ \sin\ \alpha_0 R^3}. \tag{84}$$

$$\Theta_2^0 =^q \Theta_2^0 q_3^0 +^\mu \Theta_2^0 \mu_3^0,$$

$$^q\Theta_2^0 = -\frac{(1+\nu)r_0\ \cos\ \alpha_0\ \sin\ \psi[\psi-(\psi-\sin\ \psi)\sin^2\alpha_0]}{8\pi E_M(1-\nu)\sin\ \alpha_0 R^3},$$

$$^\mu\Theta_2^0 = \frac{(1+\nu)\cos\ \psi}{4\pi E_M R^3}. \tag{85}$$

$$q_n^0 =^q q_n^0 q_3^0 +^\mu q_n^0 \mu_3^0,$$

$$
{}^{q}q_n^0 = -\frac{3\rho_0^2\{\rho_0^2\ \cos\ \psi - 2r_0^2(1-\cos\ \psi)[\cos^2\alpha_0(\psi-\sin\ \psi)\sin\ \psi + (1-\cos\ \psi)^2]\}}{16(1-\nu)R^5},
$$

$$
{}^{\mu}q_n^0 = \frac{3\rho_0^2 r_0\ \cos\ \alpha_0\ \sin\ \psi[\psi-(\psi-\sin\ \psi)\sin^2\alpha_0]}{8\ \sin\ \alpha_0 R^5}. \tag{86}
$$

$$
\mu_n^0 = {}^{q}\mu_n^0 q_3^0 + {}^{\mu}\mu_n^0\mu_3^0,
$$

$$
{}^{q}\mu_n^0 = \frac{\rho_0^2 r_0\ \cos\ \alpha_0}{16(1-\nu)\sin\ \alpha_0 R^3}\left[2(1-2\nu)\sin\ \psi(\psi+2(\sin\ \psi-\psi)\sin^2\right.
$$

$$
\left.\alpha_0)) + \frac{3(\psi+(\sin\ \psi-\psi)\sin^2\alpha_0)(2r_0^2(\sin\ \psi-\psi)(1-\cos\ \psi)+\rho_0^2\ \sin\ \psi)}{R^2}\right],
$$

$$
{}^{\mu}\mu_n^0 = \frac{3\rho_0^2}{16R^5}[2r_0^2(\psi^2\ \cos\ \psi\ \cot^2\alpha_0(2\ \cos^2\alpha_0-1)+2\psi\ \sin\ \psi\ \cos^2 \tag{87}
$$

$$
\alpha_0(1+\cos\ \psi)+(2\ \cos^2\alpha_0-1)(\cos^2\psi-1))-\rho_0^2\ \cos\ \psi].
$$

## 10. Asymptotic solution for a small radius-to-pitch ratio

Asymptotic relations presented in the previous section can undergo further simplifications. Note that there exists a set of asymptotic representations related to various directions in the space of the parameters of the problem. We present here one of the solutions which correspond to the *helix* tending to a straight line.

Let $\alpha_0$ tend to zero under a constant pitch, $l$. In this case, $r_0 \sim l\alpha_0/(2\pi) \to 0$, while the torsion $t_0 \to 2\pi/l$ = const; thus, the *helix* tends to a straight line. However, the normal, $\boldsymbol{n}$, which coincides with the external forces and moments,

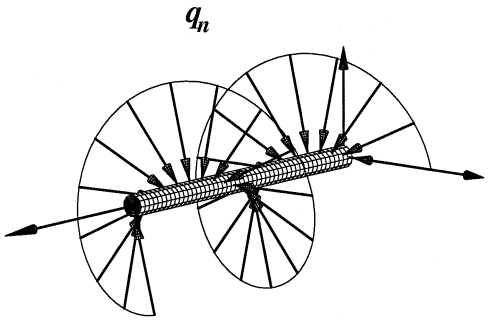


Fig. 7. The normal rod–matrix interaction force $q_n$ for the case when the fiber becomes almost rectilinear.

forms a screw surface as in the case of a 'genuine' *helix* (Fig. 7). In this case, the asymptotic fields in the matrix can be obtained based on the superposition of the fundamental fields induced by the forces and moments distributed along a straight line, but directed in accordance with its nonzero torsion. Note that the rod, which possesses a bending stiffness, cannot be straightened out completely by bounded tensile forces even in the case of a free rod without a surrounding matrix. In this real case, the torsion of the *helix* is single-valued — in contrast to the idealization adopted in this subsection, where the limiting value of the torsion is considered. This idealization is used here to simplify the determination of the fields in the matrix while the internal forces in the rod are calculated for nonzero $\alpha_0$ and $r_0$.

Under the condition $\alpha_0 \ll 1$, the first term in the expression for the distance $R$, Eq. (83) is relatively small

$$\frac{2r_0^2(1-\cos\ \psi)}{s^2\ \cos^2\alpha_0} = \frac{2r_0^2(1-\cos\ \psi)\sin^2\alpha_0}{\psi^2 r_0^2\ \cos^2\alpha_0} \leq \frac{\sin^2\alpha_0}{\cos^2\alpha_0} \ll 1, \tag{88}$$

and the distance can be represented as follows:

$$R^2 = s^2 + \rho_0^2 \quad (\alpha_0 \ll 1). \tag{89}$$

The force/moment and displacement/rotation relations can now be expressed based on the relation (89). This can be done in two ways: firstly, by a simplification of the expressions (84)–(87) under the conditions $\alpha_0 \to 0$, $\psi = s \sin \alpha_0/r_0 \to 2\pi s/l$ and $r_0/l = 2\pi \tan \alpha_0 \to 0$; secondly, by considering the rod to be straight in its actual state. Both approaches, after integration with respect to $s$, in accordance with Eqs. (63) and (64), lead to the same asymptotes, namely:

$$^{q}U_n = \frac{1+\nu}{8\pi E_M(1-\nu)}[2(3-4\nu)K_0(t_0\rho_0) + t_0\rho_0 K_1(t_0\rho_0)],$$

$$^{\mu}U_n = -\frac{(1+\nu)t_0}{2\pi E_M}K_0(t_0\rho_0), \tag{90}$$

$$^{q}\Theta_n = -\frac{(1+\nu)t_0}{4\pi E_M(1-\nu)}K_0(t_0\rho_0), \quad ^{\mu}\Theta_n = \frac{(1+\nu)t_0}{2\pi E_M\rho_0}K_1(t_0\rho_0), \tag{91}$$

$$^{q}q_n = -\frac{1-2\nu}{2(1-\nu)}t_0\rho_0 K_1(t_0\rho_0) - \frac{1}{4(1-\nu)}t_0^2\rho_0^2 K_2(t_0\rho_0),$$

$$^{\mu}q_n = \frac{3}{4}t_0^2\rho_0 K_1(t_0\rho_0), \tag{92}$$

$$^{q}\mu_n = -\frac{\rho_0}{4(1-\nu)}[(1-2\nu)t_0\rho_0 K_0(t_0\rho_0) + t_0^2\rho_0^2 K_1(t_0\rho_0)],$$

$$^{\mu}\mu_n = \frac{1}{4}t_0^2\rho_0^2K_0(t_0\rho_0) - \frac{1}{4}t_0\rho_0K_1(t_0\rho_0) + \frac{1}{4}t_0^2\rho_0^2K_2(t_0\rho_0), \tag{93}$$

where $K_0(t_0\rho_0)$, $K_1(t_0\rho_0)$ and $K_2(t_0\rho_0)$ are the modified Hankel functions.

Note that these expressions are to be substituted in the system of Eqs. (66), (69)–(71), where the curvature $\kappa_0$ is not assumed to be zero. The relations (90)–(93) yield a parametric representation of the 'helical elastic foundation' as a generalization of the Winkler foundation. The helical foundation is then introduced in the equilibrium equations of the rod. As can be seen in Fig. 16 this asymptotic representation of the helical foundation shows rather good accuracy even for $\alpha_0 = \pi/6$ and $r_0 \gg \rho_0$.

The asymptotic relations (90)–(93) can be further simplified for the case $t_0\rho_0 \ll 1$. In this case, using well-known expansions for Hankel functions, one obtains:

$$^{q}U_n = \frac{1+\nu}{8\pi E_M(1-\nu)}[2(3-4\nu)(\gamma - \ln(2)) - 1 + 2(3-4\nu)\ln(t_0\rho_0)],$$

$$^{\mu}U_n = -\frac{(1+\nu)t_0}{2\pi E_M}(\ln(2) - \gamma - \ln(t_0\rho_0)), \tag{94}$$

$$^{q}\Theta_n = -\frac{(1+\nu)t_0}{4\pi E_M(1-\nu)}(\ln(2) - \gamma - \ln(t_0\rho_0)), \quad ^{\mu}\Theta_n = \frac{(1+\nu)}{2\pi E_M\rho_0^2}, \tag{95}$$

$$^{q}q_n = -1 \quad ^{\mu}q_n = \tfrac{3}{4}t_0, \tag{96}$$

$$^{q}\mu_n = -\frac{\rho_0^2t_0}{4(1-\nu)}[(1-2\nu)(\ln(2) - \gamma - \ln(t_0\rho_0)) + 1], \tag{97}$$

$$^{\mu}\mu_n = \tfrac{1}{4}t_0^2\rho_0^2(\ln(2) - \gamma - \ln(t_0\rho_0)). \tag{98}$$

In these formulas (and only here!), $\gamma$ is the Euler constant.

## 11. Inextensible rod

Consider a simplified formulation of the problem, where the helical inclusion is assumed to be inextensible. In this case, a relation between the initial radius of the *helix*, $r_0^i$, and its actual value, $r_0$, can be obtained explicitly. From Eqs. (31), (33) and from the condition of inextensibility, $\lambda_s \equiv 1$ it follows that

$$r_0^2 = r_0^i\frac{1 - \lambda_x^2\ \cos^2\alpha_0^i}{\kappa_0^i + 2t_0^ir_0^i\lambda_x\gamma + \cos^2\alpha_0^ir_0^i\lambda_x^2\gamma^2}, \tag{99}$$

$$r_0 = \frac{r_0^i}{\sin\ \alpha_0^i}\sqrt{1-\lambda_x^2\ \cos^2\alpha_0^i}, \quad (\gamma = 0). \tag{100}$$

Based on Eq. (31) an explicit relation can also be obtained for the angle $\alpha_0$:

$$\cos\ \alpha_0 = \lambda_x\ \cos\ \alpha_0^i. \tag{101}$$

The distributions $q_3^0$ and $\mu_3^0$ can then be easily found using the Eqs. (66) and (69). Finally, the internal tensile and shear forces can be obtained from Eqs. (70) and (71).

## 12. Numerical procedure and discussion

The procedure which was carried out in calculating the fields in the matrix, the rod/matrix interaction and the forces and moments in the rod, is systematically described here [3].

The starting point of the procedure is Kelvin's fundamental solution for displacements (55) and stresses (56) induced by the unit concentrated force $q_3^0$ and moment $\mu_3^0$ given in the *H*-system. In order to calculate displacements and the angle of rotation of the cross-section of the rod as well as the distributed force and moment acting on the rod cross-section, these components were transformed to the *helix*-associated *TC*-system according to Eqs. (58) and (A6). The averaging of the displacement and stress components over the cross-section interface was carried out according to Eqs. (59)–(62). These averaged components, namely, the displacement in the normal direction $U_n^0$, the angle of rotation of the cross-section of the rod $\Theta_2^0$, the distributed force $q_n^0$ and the moment $\mu_n^0$ were then integrated over the domain $(-\infty < s < \infty)$ along the *helix*. As the structure of the integrands in Eqs. (59)–(62) does not permit an analytic calculation of these integrals, a double numerical integration is inevitable. In integrating over the *s*-domain, in the central section of the integration path, $s \in [-s^*, s^*]$, where $s^*$ is large enough, the integrals were calculated numerically. For $|s| > s^*$, asymptotic expressions for integrands were used, thus leading to analytic integration. The accuracy of the integration was controlled by an adaptive procedure in which a proper choice of the value of $s^*$ leads to the required tolerance.

As was noted in Section 8, the distance $R$ can be assumed to be $\phi$-independent if the condition Eq. (12) is valid. In this case all the integrals with respect to $\phi$, Eqs. (59)–(62), were calculated analytically thus requiring only numerical integration with respect to $s$.

At the next stage, the equilibrium equations of the rod and the continuity conditions of the radial and angular displacements on the rod/matrix interface were used. The final system consists of three nonlinear equations, (69)–(71), with respect to $q_n$, $\mu_n$ and the shear force $B$. The solution of this system gives the

[3] All calculations were performed using the symbolic computation system, "Maple".

unknown distributions $q_n$, $\mu_n$ and the shear force in the rod. These values were then substituted back to Eqs. (43)–(45), thus yielding the internal forces and moments in the rod as well as its deformation.

Note that the results obtained are expressed in terms of the deformed state of the composite, and the initial state is only determined in the final step of the solution. However, the initial state and not the final state is known in advance. The determination of the latter is the problem. This 'straightforward' way is not directly applicable here. The difficulties are caused by the fact that all equilibrium equations of the nonlinear problem considered are expressed in terms of the deformed state. In order to avoid this obstacle, one may use the method of incremental linearization. In this case, at each step in the formulation of the equilibrium equations, the difference between two neighboring states can be neglected.

Numerical results are presented for axial extension of the composite. The influence of the matrix-to-rod elastic moduli ratio on the radial strain of the *helix*-associated cylinder (shown in Fig. 5) is presented in Fig. 8 for various values of the matrix-to-rod ratio of the elastic moduli. The influence of the same ratio on the tensile force in the rod is shown in Fig. 9. We observe that as $E_m/E_r$ increases, the relations become increasingly linear.

An important geometrical parameter is the helical angle. Its influence on the tensile force in the rod is shown in Fig. 10. Variation of the angle leads to the corresponding variation of the effective elastic modulus of the rod in an initial

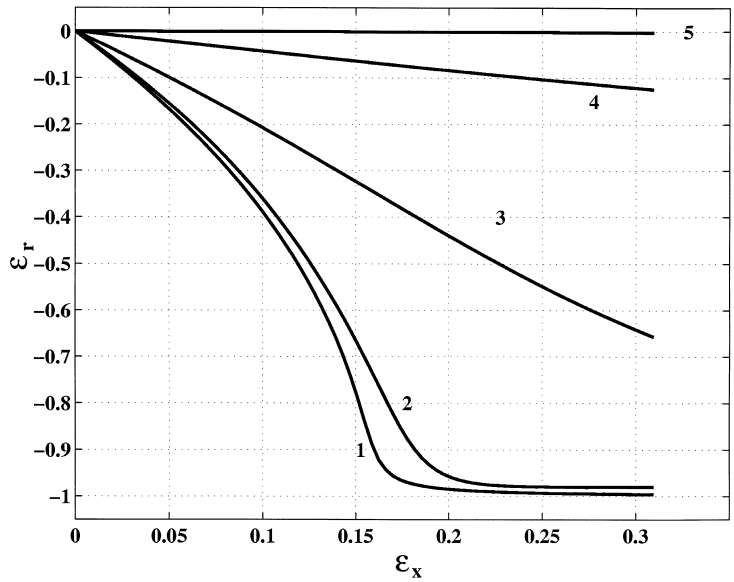


Fig. 8. Radial strain, $\epsilon_r = r_0/r_0^i - 1$, for the case $\alpha_0 = \pi/6$, $\rho_0/r_0 = 0.1$: (1) a free rod, $E_M = 0$; (2) $E_M/E = 0.001$; (3) $E_M = 0.001$; (4) $E_M/E = 0.01$; (5) $E_M/E = 1$.

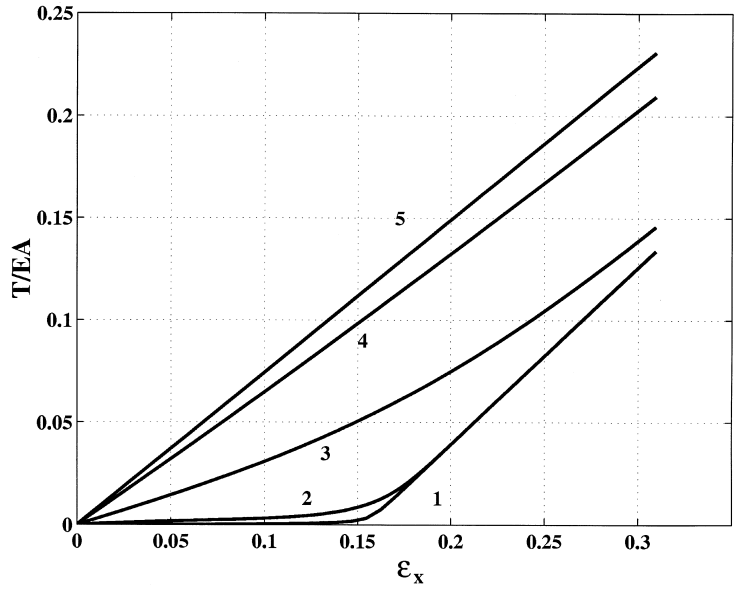


Fig. 9. Normalized tensile force in the rod, $T/EA$, for the case $\alpha_0=\pi/6$, $\rho_0/r_0=0.1$: (1) a free rod, $E_M=0$; (2) $E_M/E=0.001$; (3) $E_M=0.001$; (4) $E_M/E=0.01$; (5) $E_M/E=1$.

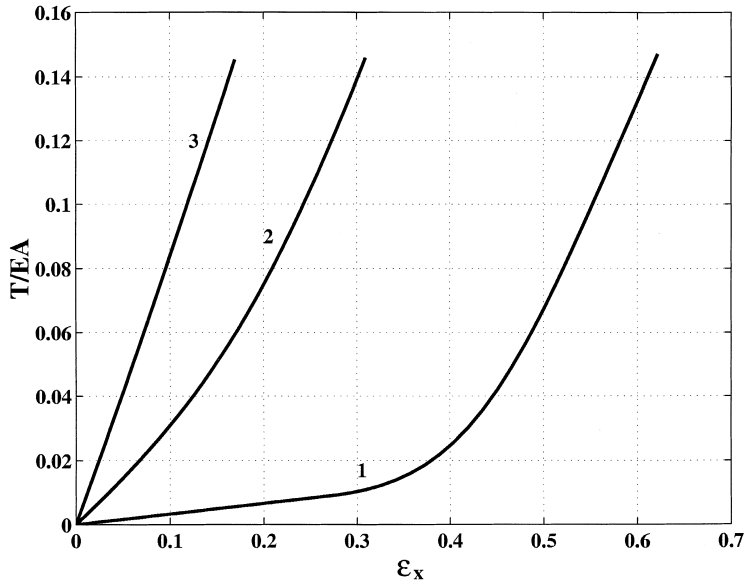


Fig. 10. Normalized tensile force in the rod $T/EA$ for the case $\rho_0/r_0=0.1$, $E_M/E=0.001$: (1) $\alpha_0=\pi/4$; (2) $\alpha_0=\pi/6$; (3) $\alpha_0=\pi/12$.

portion of its axial strain. An increase in the angle leads to a decrease in the modulus and to an increase in the hardening-type nonlinearity of the stress–strain relation.

The presence of the helical inclusion which causes an additional resistance to deformation relative to the resistance of the undisturbed matrix was calculated by the following procedure. Using the method of incremental linearization, the additional strain energy of the matrix, $W_m$, per unit length in the $x$-direction is first calculated:

$$W_m = \frac{1}{\cos\ \alpha_0}\left(\int_0^{U_n} q_n\ \mathrm{d}U_n + \int_0^{\Theta_n} \mu_n\ \mathrm{d}\Theta_n\right). \tag{102}$$

Noting that the strain energy of the rod per unit length in the $x$-direction is

$$W_r = \frac{EA\epsilon_s^2 + EI(\kappa_0 - \kappa^i)^2 + GI_p(t_0 - t_0^i)^2}{2\ \cos\ \alpha_0}, \tag{103}$$

the total additional energy per unit length is

$$W = W_r + W_m. \tag{104}$$

Using this result the additional resistance was calculated. In the case of an axial extension, the total additional tensile force is

$$T_{\text{total}} = \frac{\partial W}{\partial \epsilon_x}. \tag{105}$$

The total inclusion-associated axial force versus axial extension is presented in Figs. 11 and 12. As can be seen in Fig. 12, the matrix-associated axial force (additional to the non-disturbed forces in the matrix) caused by the presence of the helical rod is considerable in spite of a relatively low modulus of the matrix.

The near-rod stress fields in the matrix are shown in Figs. 13 and 14. These results demonstrate that the stresses are mainly concentrated in a close vicinity of the rod and decay rapidly with the radial distance.

Comparisons of straight, nonzero-torsion-rod asymptotic results and the results corresponding to the spherical-model-based Winkler foundation [4] — with the 'exact' solutions are presented in Figs. 15 and 16. The exact solutions corresponding to the general formulation adopted in this paper and the asymptote based on the inequality (12) were so close that they cannot be distinguished in the presented plots.

In Fig. 17, the expected tensile force in the rod under fracture of the matrix is

[4] Consider a rigid sphere embedded in the matrix. A force to sphere diameter ratio as a function of the sphere displacement represents the 'spherical elastic foundation' which could be used for a rough estimation of the helical foundation. In this model, the interaction force and moment are $q_n = E_M(r_0 - r_0^i)$, $\mu_n = 0$.

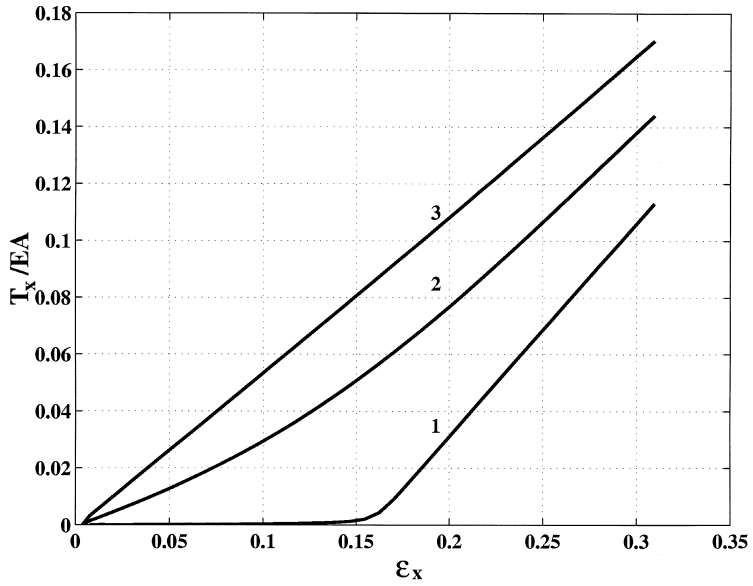


Fig. 11. Normalized inclusion-associated axial tensile force, $T_x/EA$, for the case $\alpha_0=\pi/6$, $\rho_0/r_0=0.1$: (1) a free rod, $E_M=0$; (2) $E_M/E = 0.001$; (3) $E_M/E = 0.01$ and $E_M/E = 0.1$. (Note: the difference of results for these two cases is too small to be seen in the figure.)

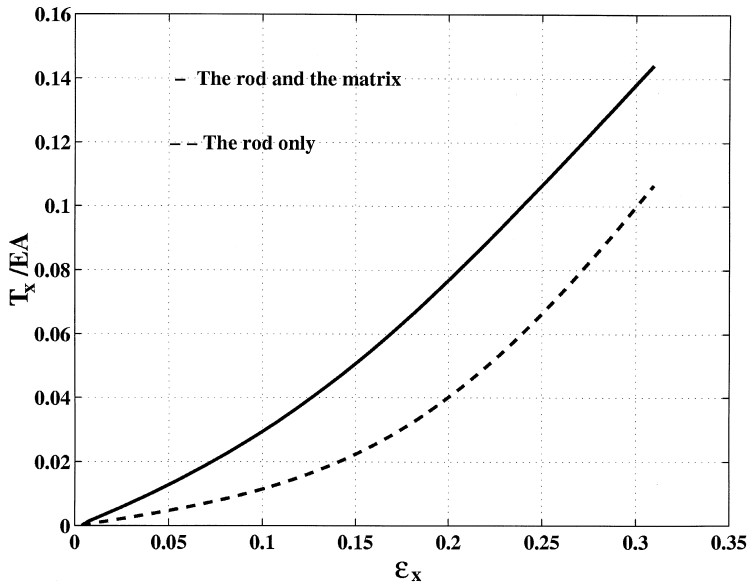


Fig. 12. Contribution of matrix to additional resistance of the composite due to presence of the inclusion: $\alpha_0=\pi/6$, $\rho_0/r_0=0.1$; $E_M/E = 0.001$.

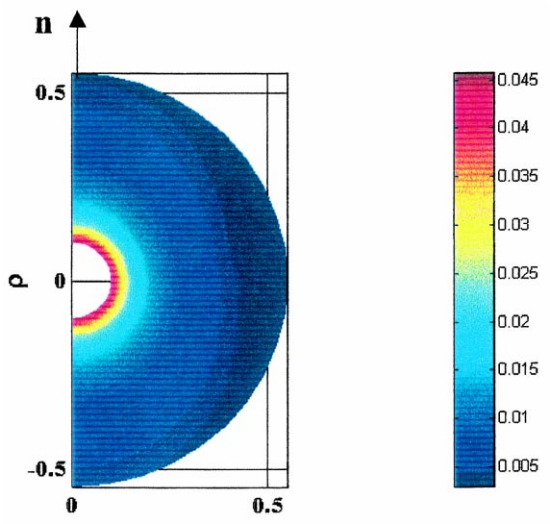


Fig. 13. Normalized octahedral stress, $\sigma_0/E_M$, in the matrix in the plane of the rod cross-section: $\alpha_0=\pi/6$, $\rho_0/r_0=0.1$; $E_M/E = 0.001$.

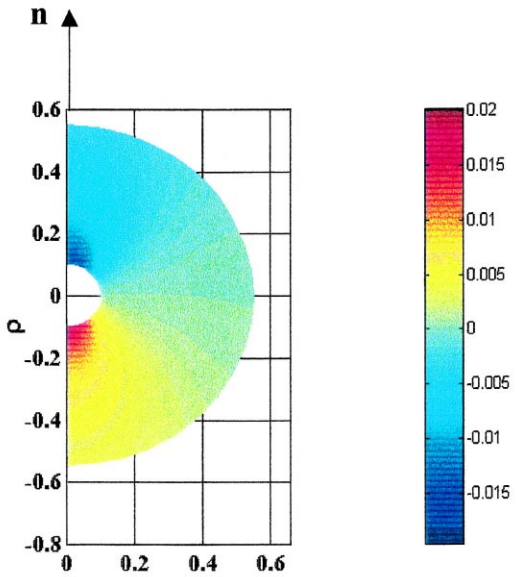


Fig. 14. Normalized stress $\sigma_{22}/E_M$ in the matrix in the plane of the rod cross-section: $\alpha_0=\pi/6$, $\rho_0/r_0=0.1$; $E_M/E = 0.01$.

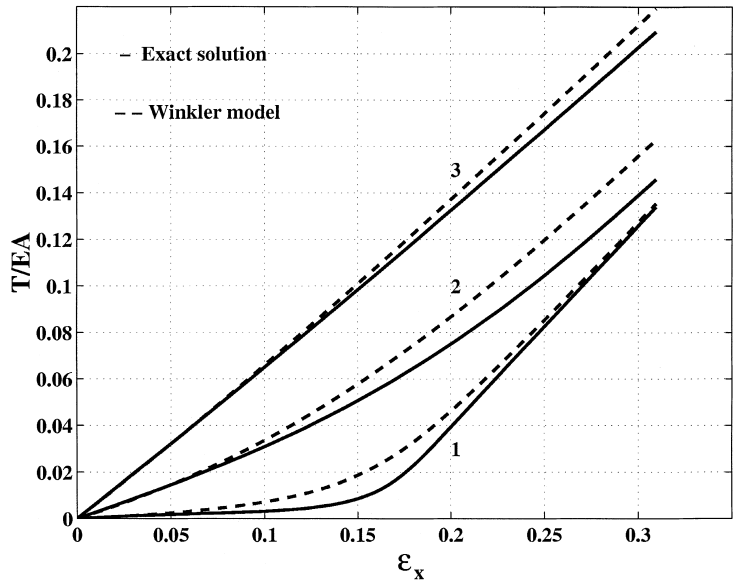


Fig. 15. Normalized tensile force in the rod, $T/EA$, for the case $\alpha_0=\pi/6$, $\rho_0/r_0=0.1$: (1) $E_M/E = 0.0001$; (2) $E_M/E = 0.001$; (3) $E_M/E = 0.01$. Dotted curves correspond to the simplified model, where the rod/matrix interaction is considered as in the case of the Winkler spherical-model-based elastic foundation.

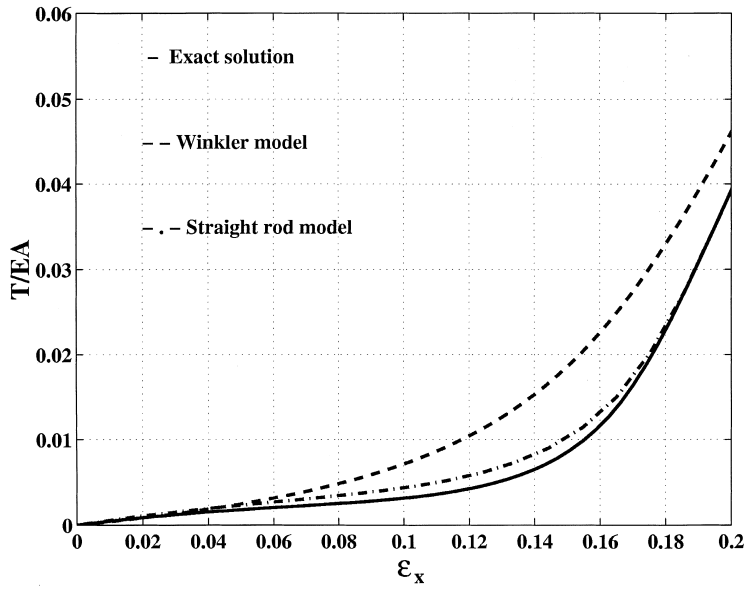


Fig. 16. Normalized tensile force in the rod, $T/EA$, for the case $\alpha_0=\pi/6$, $\rho_0/r_0=0.1$; $E_M/E = 0.001$ and different simplified models of the rod/matrix interaction.

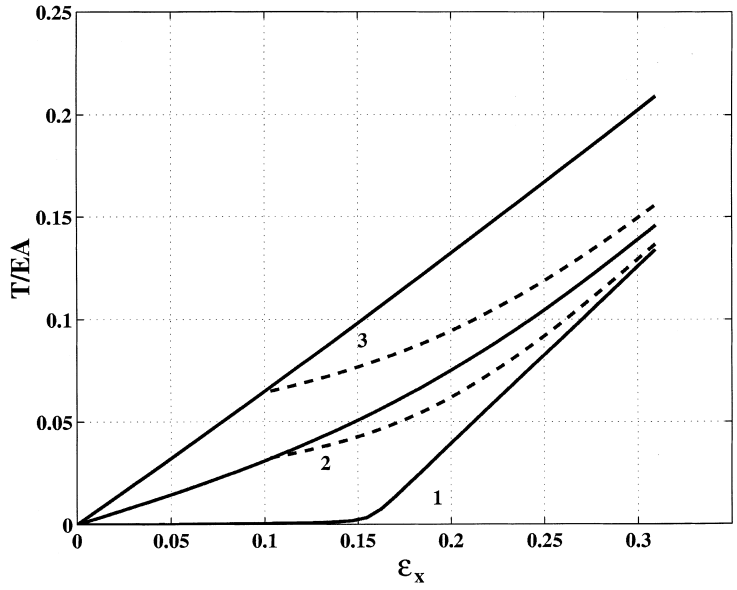


Fig. 17. Normalized tensile force in the rod, $T/EA$, for the case $\alpha_0=\pi/6$, $\rho_0/r_0=0.1$: (1) a free rod, $E_M=0$; (2) $E_M/E = 0.001$; (3) $E_M/E = 0.1$. Dotted curves correspond to the case of fracture of the matrix.

shown. It is assumed that during fracture when the rod is cutting the matrix the resistance to the normal displacement of the rod toward the *helix* axis is constant, the same as at initiation of fracture. It can be seen that the axial extension is still stable during such fracture.

## Acknowledgements

This research was supported by Grant Nos 9673-3-98 and 1207-1-98 from the Ministry of Science, Israel.

## Appendix. Relations between the coordinate systems

In the *TC*-system, the position vector, $\boldsymbol{R}(s, \rho, \phi)$, has the following expression:

$$\boldsymbol{R}(s, \rho, \phi) = \boldsymbol{R}(s, 0) + \rho(\boldsymbol{n} \cos \phi + \boldsymbol{b} \sin \phi). \tag{A1}$$

The vector $\boldsymbol{R}(s, 0) \equiv \boldsymbol{R}(s, 0, \phi)$, which defined a point on the *helix*, and the corresponding components of the Frenet triad (2)–(4) have the following expressions in the *X*-system:

$$\boldsymbol{R}(s, 0) = s \cos \alpha_0 \boldsymbol{k}_1 + r_0(\cos \psi \boldsymbol{k}_2 + \sin \psi \boldsymbol{k}_3),$$

$$\boldsymbol{\tau} = \cos\ \alpha_0 \boldsymbol{k}_1 - \sin\ \alpha_0(\sin\ \psi \boldsymbol{k}_2 - \cos\ \psi \boldsymbol{k}_3),$$

$$\boldsymbol{n} = -\cos\ \psi \boldsymbol{k}_2 - \sin\ \psi \boldsymbol{k}_3,$$

$$\boldsymbol{b} = \sin\ \alpha_0 \boldsymbol{k}_1 + \cos\ \alpha_0(\sin\ \psi \boldsymbol{k}_2 - \cos\ \psi \boldsymbol{k}_3),$$

$$\psi = \frac{s\ \sin\ \alpha_0}{r_0} = \frac{x\ \tan\ \alpha_0}{r_0}. \tag{A2}$$

It follows immediately that the $X$-coordinates are expressed as

$$x_1 = s\ \cos\ \alpha_0 + \rho\ \sin\ \phi\ \sin\ \alpha_0,$$

$$x_2 = r_0\ \cos\ \psi - \rho(\cos\ \phi\ \cos\ \psi - \sin\ \phi\ \sin\ \psi\ \cos\ \alpha_0),$$

$$x_3 = r_0\ \sin\ \psi - \rho(\cos\ \phi\ \sin\ \psi + \sin\ \phi\ \cos\ \psi\ \cos\ \alpha_0). \tag{A3}$$

The $H$-coordinates are

$$\xi_1 = x - s\ \cos\ \alpha_0 = b\ \sin\ \alpha_0 = \rho\ \sin\ \phi\ \sin\ \alpha_0,$$

$$\xi_2 = -x_2\ \sin\ \psi + x_3\ \cos\ \psi = -b\ \cos\ \alpha_0 = -\rho\ \sin\ \phi\ \cos\ \alpha_0,$$

$$\xi_3 = r_0 - x_2\ \cos\ \psi - x_3\ \sin\ \psi = n = \rho\ \cos\ \phi. \tag{A4}$$

Consider a point $(0, \rho_0, \phi)$ in the $TC$-system. Its coordinates in the $X$-system are

$$x_1 = \rho_0\ \sin\ \phi\ \sin\ \alpha_0,$$

$$x_2 = r_0 - \rho_0\ \cos\ \phi,$$

$$x_3 = -\rho_0\ \sin\ \phi\ \cos\ \alpha_0. \tag{A5}$$

Consider now two points: $(0, \rho_0, \phi)$ and $(s, 0)$. The first point has the following coordinates in the $H$-system with the origin at the second point:

$$\xi_1 = -s\ \cos\ \alpha_0 + x = -s\ \cos\ \alpha_0 + \rho_0\ \sin\ \alpha_0\ \sin\ \phi,$$

$$\xi_2 = -x_2\ \sin\ \psi + x_3\ \cos\ \psi = -r_0\ \sin\ \psi + \rho_0(\cos\ \phi\ \sin\ \psi - \sin\ \phi\ \cos\ \psi\ \cos\ \alpha_0),$$

$$\xi_3 = r_0 - x_2 \cos\psi - x_3 \sin\psi = r_0(1-\cos\psi) + \rho_0(\cos\phi\cos\psi + \sin\phi\sin\psi\cos\alpha_0). \tag{A6}$$

Consider a point $(x, r, \theta)$ in the $C$-system. Its coordinates in the $H$-system (with the above defined origin) are

$$\xi_1 = x - s\cos\alpha_0,$$

$$\xi_2 = r\sin(\theta-\psi),$$

$$\xi_3 = r_0 - r\cos(\theta-\psi). \tag{A7}$$

Let $\boldsymbol{k}_m$ (for the $X$-system: $x_1 = x, x_2, x_3$), $\boldsymbol{c}_m$ (for the $C$-system: $x, r, \theta$), $\boldsymbol{t}_m$ (for the $T$-system: $s = 0, n, b$), and $\boldsymbol{h}_m$ (for the $H$-system: $\xi_1, \xi_2, \xi_3$, with the origin at the second point, $s$, as was defined above) be the unit vectors related to the corresponding systems with one exception: $\boldsymbol{t}_1$ is directed along $\boldsymbol{\tau}$, that is, not along $s$ for $r \neq r_0$; thus $\boldsymbol{t}_m$ represents a local rectangular system. If $\alpha_{ml} = \boldsymbol{k}_m\boldsymbol{h}_l$, the spin matrix $A = [\alpha_{ml}]$, which defines the rotation around the $x$-axis by an angle $-(\pi/2+\psi)$, is

$$A = \begin{bmatrix} 1 & 0 & 0 \\ 0 & -\sin\psi & \cos\psi \\ 0 & -\cos\psi & -\sin\psi \end{bmatrix}. \tag{A8}$$

If $\beta_{ml} = \boldsymbol{c}_m\boldsymbol{h}_l$, the spin matrix $B = [\beta_{ml}]$, which defines the rotation around the $x$-axis by an angle $-(\pi/2+\psi-\theta)$, is

$$B = \begin{bmatrix} 1 & 0 & 0 \\ 0 & \sin(\theta-\psi) & \cos(\theta-\psi) \\ 0 & -\cos(\theta-\psi) & \sin(\theta-\psi) \end{bmatrix}. \tag{A9}$$

Finally, if $\gamma_{ml} = \boldsymbol{t}_m\boldsymbol{h}_l$, the spin matrix $C = [\gamma_{ml}]$ defines a rotation around the $x$-axis by the angle $-(\pi/2+\psi)$, followed by a rotation about the $t_2$-axis by the angle $\alpha_0$. This is the transformation from the $H$-system with the origin at a point $s$ on the *helix* to the $T$-system:

$$C = \begin{bmatrix} \cos\alpha_0 & \sin\alpha_0\cos\psi & -\sin\alpha_0\sin\psi \\ 0 & \sin\psi & \cos\psi \\ \sin\alpha_0 & -\cos\alpha_0\cos\psi & \cos\alpha_0\sin\psi \end{bmatrix}. \tag{A10}$$

These dependencies are used in the determination of displacement and stress fields in the matrix.

## References


Aboudi, J., 1991. Mechanics of Composite Materials — A Unified Micromechanical Approach. Elsevier, New York.

Breig, W.F., 1991. Finite element analysis of spiral hose utilizing laminate theory. SAE (Society of Automotive Engineers) Transactions 100 (5), 968–986.

Bustamante, C., Marko, J.F., Siggia, E.D., Smith, S., 1994. Entropic elasticity of $x$-phase DNA. Science 265, 1599–1600.

Butterworth, D., 1992. Developments in shell-and-tube exchangers. Proceeding of the 3rd UK National Conference incorporating 1st European Conference on Thermal Sciences, Birmingham, England, 16–18 September 1992. Institution of Chemical Engineers Symposium Series, vol. 1(129). Published by the Institute of Chemical Engineers, Davis Building, Rugby, England, pp. 409–415.

Cardou, A., Jolicoeur, C., 1997. Mechanical models of helical strands. Applied Mechanics Reviews 50 (1), 1–14.

Cherkaev, A.V., Slepyan, L.I., 1995. Waiting element structures and stability under extension. Int. J. of Damage Mech. 41, 58–82.

Chiskis, A., Parnes, R., 1998. Nonlinear effects in the extension of an elastic space containing a wavy layer inclusion. J. Mech. Phys. Solids 46, 1213–1251.

Chiskis, A., Parnes, R., Slepyan, L., 1997. Nonlinear behavior of wavy composite under tension. J. Mech. Phys. Solids 45, 1357–1392.

Chou, T.W., 1992. Microstructural Design of Fiber Composites. Cambridge University Press, Cambridge.

Christensen, R.M., 1979. Mechanics of Composite Materials. Wiley, New York.

Dong, J.L., Hee, C.K., Byoung, G.M., 1996. Development of a new blood pump using a shape memory alloy actuator. ASAIO Journal 24 (5), M765–M768.

Ergashov, M., 1992. Study of the propagation of elastic waves in wound structures taking into account their rotation under extension. Applied Math. and Mech. 56 (1), 117–124 [English translation of Prikladnaya Matematika i Mekhanika].

Foral, R.F., 1989. Delamination failures in curved composite laminates. Key Engineering Materials 37, 137–148.

Fujiki, Michiya, 1996. Helix provides new insights — a bridge between inanimate polymers created with silicon atoms and the homochiral living world. NTT R. and D. 45 (7), 678–687.

Fung, Y.C., 1965. Foundations of Solid Mechanics. Prentice-Hall.

Ge, Fuding, Zhu, Jing, Chen, Limin, 1996. Quantitative study of effective parameters of chiral composite material. International Journal of Infrared and Millimeter Waves 17 (8), 1457–1463.

Grum-Grzhimajlo, N.A., Vaninskij, V.M., Korolev, M.V., Umerkin, G. Kh, 1995. Production of pipes of new types-spirally welded self-expansion pipes for heat lines. Tyazheloe Mashinostroenie 5, 17–18.

Serruys, P.W. (Ed.), 1997. Handbook of Coronary Stents. Martin Dunitz, London.

Hashin, Z., 1983. Analysis of composite materials. Journal of Applied Mechanics 50, 481–505.

Iwata, M., Isoda, T., Itoh, T., 1994. Processing of continuous fiber reinforced Si//3N//4 matrix composites for gas turbine engine components. In: Proceedings of the International Gas Turbine and Aeroengine Congress and Exposition, ASME, New York, USA, pp. 1–8.

Kagawa, Y., Nakata, E., Yoshida, S., 1982. Fracture behavior and toughness of helical fiber reinforced composite metals. In: Hayashi, T., Kawata, K., Umekawa, S. (Eds.), Progress in Science and Engineering of Composites. ICCM-IV, Tokyo, pp. 1457–1464.

Kautz, H.E., 1987. Ultrasonic evaluation of mechanical properties of thick, multilayered, filament-wound composites. Materials Evaluation 45 (12), 1404–1412.

Kobe, J.M., Wiest, J.M., 1993. Finitely extensible bead-string chain macromolecules in steady elongation flows. Journal of Rheology 37 (5), 947–960.

Kohkoner, K.E., Anderson, S., Strong, A.B., 1991. Machining graphite composites with polycrystalline diamond end mills. Proceedings of the 23rd International SAMPE Conference, Kiamesha Lake,

NY, USA, 21–24 October 1991. International SAMPE Technical Conference, vol. 23. Published by SAMPE, Covina, CA, USA, pp. 1036–1046.

Krylov, V., Rosenau, Ph, 1996. Solitary waves in an elastic string. Physics Letters A 217, 31–42.

Krylov, V., Slepyan, L.I., 1997. Binary wave in a helical fiber. Physical Review B 55 (21), 14067–14070.

Krylov, V., Parnes, R., Slepyan, L.I., 1998. Nonlinear waves in an inextensible flexible helix. Wave Motion 27, 117–136.

Lhermitte, T., Perrin, B., Fink, M., 1989. Dispersion relations in elastic shear waves in cross-ply fiber reinforced composites. Ultrasonics Symposium Proceedings, vol. 2. Published by IEEE, IEEE Service Center, Piscataway, NJ, USA (IEEE cat. no. 89CH2791-2), pp. 1175–1179.

Li, Shihong, Zhang, Ronghui, Fu, Shaoyun, Chen, Xin, Zhou, Belian, Zeng, Qiyun, 1994. Biomimetic model of fiber-reinforced composite materials. Journal of Materials Science and Technology 10 (1), 34–38.

Lindell, I.V., Shivola, A.H., Tretyakov, S.A., Viitanen, A.J., 1994. Electromagnetic Waves in Chiral and Bi-isotropic Media. Artech House, Boston.

Mariotte, F., Tretyakov, S.A., Sauviac, B., 1996. Modeling effective properties of chiral composites. IEEE Antennas and Propagation Magazine 38 (2), 22–32.

Meille, S.V., Allegra, G., 1996. Chiral crystallization of helical polymers. Proceedings of the 1996 ACS Orlando Meeting, Orlando, FL, USA, 25–29 August. Polymer Preprints, Division of Polymer Chemistry (American Chemical Society), vol. 37(2), pp. 426–427.

Morris, D.H., Harris, C.E., 1989. Predicting strength of filament-wound specimens with surface cuts. Proceedings of the 34th International SAMPE Symposium and Exhibition — Tomorrow's Materials: Today, Reno, NV, USA, 8–11 May 1989. International SAMPE Symposium and Exhibition. Book 1 (of 2), SAMPE, Covina, CA, USA, pp. 1120–1129.

Navi, P., Huet, C., 1989. Three dimensional multilevel technique to study influence of the fiber microstructure on wood macroscopic elastic properties. AMD (Sympopsia Series) (American Society of Mechanical Engineers, Applied Mechanics Division), vol. 99. Published by American Society of Mechanical Engineers (ASME), New York, NY, USA, pp. 61–67.

Okamoto, Y., Nakano, T., 1996. Stereo specific and helix-sense-sensitive radical polymerizations of methacrylates. Proceedings of the 1996 ACS Orlando Meeting, Orlando, FL, USA, 25–29 August 1996. Polymer Preprints, Division of Polymer Chemistry, American Chemical Society, vol. 37(2), pp. 444–445.

Padros, N., Ortigosa, J.I., Baker, J., Iskander, M.F., Thornberg, B., 1997. Comparative study of high-performance GPS receiving antenna designs. IEEE Transactions on Antennas and Propagation 45 (4), 698–706.

Pathak, S.K., Singh, S.P., 1996. Field analysis of a tape helix with embedded bio-media for microwave hyperthermia. Journal of Medical Engineering and Technology 20 (1), 24–33.

Petryl, M., Hert, J., Fiala, P., 1996. Spatial organization of the haversian bone in man. Journal of Biomechanics 29 (2), 161–169.

Pistol'kors, A.A., Bakhrakh, L.D., Kurochkin, A.P., 1995. Development of Russian antenna engineering. Radiotekhnika 40 (7-8), 26–41.

Rabin, Y., Korin, E., 1996. Incorporation of phase-change materials into a ground thermal energy storage system: theoretical study. Journal of Energy Resources Technology, Transactions of the ASME 118 (3), 237–241.

Savenkov, V.N., Solodova, L.A., 1988. State of stress and strain of a multilayered composite flexible pipe reinforced by helical carcass. Mechanics of Composite Materials 23 (6), 762–768 [English translation of Mekhanika Kompozitnykh Materialov].

Shen, I.Y., Guo, W., Pao, Y.C., 1997. Torsional vibration control of a shaft through active constrained layer damping treatments. Journal of Vibration and Acoustics 119, 504–511.

Shewbridge, S.E., Sousa, J.B., 1991. Dynamic properties of reinforced sand. Journal of Geotechnical Engineering 117 (9), 1402–1422.

Slepyan, L.I., Krylov, V., Parnes, R., 1995a. Solitary waves in an inextensible, flexible, helicoidal fiber. Physical Review Letters 74 (14), 2725–2728.

Slepyan, L.I., Krylov, V., Parnes, R., 1995b. Solitary wave in a helix. Proc. Estonian Acad. Sci. Phys. Math. 44, 29–39.

Slepyan, L., Krylov, V., Rosenau, Ph, 1998. Solitary waves in a flexible, arbitrary elastic helix. J. Engng Mech. 124 (9), 966–970.

Smith, S.B., Finzi, L., Bustamante, C., 1992. Direct mechanical measurements of elasticity of single DNA molecules by using magnetic beads. Science 258, 1122–1126.

Watkins, D.A., Ash, E.A., 1954. The helix as a backward-wave circuit structure. Journal of Applied Physics 25 (6), 782–790.

Williams, F.W., Howson, W.P., Banerjee, J.R., 1993. Natural frequencies of members with coupled extensional torsional motion. A physical approach. Journal of Sound and Vibration 165 (2), 373–375.

Zhang Zhibin, 1997. Prediction of Young's modulus of steel cord under compression. Proceedings of the 1997 67th Annual Convention, Atlanta, GA, USA, 7–9 April 1997. Proceedings of the Annual Convention of the Wire Association International, pp. 75–82.